Sub-Doppler Cooling of Fermionic Lithium

A master thesis submitted to the
FACULTY OF
MATHEMATICS, COMPUTER SCIENCE AND PHYSICS,
OF THE LEOPOLD-FRANZENS UNIVERSITY OF INNSBRUCK

in partial fulfillment
of the requirements for the degree of

MASTER OF SCIENCE

carried out at the Institute for Quantum Optics and Quantum Information, and
the Institute for Experimental Physics at the University of Innsbruck
under the supervision of Univ.-Prof. Dr. Rudolf Grimm

presented by
ISABELLA FRITSCHE BSC

JUNE 2015

Abstract

In our experimental approach to prepare strongly interacting Li-K mixtures, fermionic ^{6}Li acts as the cooling agent. The high temperature of ^{6}Li in the standard magneto-optical trap (MOT), operated on the D2 transition, limits the efficiency. To overcome this limitation, we implement a gray molasses cooling scheme on the D1 transition to reach sub-Doppler temperatures. In this technique, cooling arises from the Sisyphus effect in combination with a sharp cooling feature near the Raman transition where the two ground states ($F = 1/2$ and $F = 3/2$) are coupled via two lasers, blue detuned from the $F' = 3/2$ excited state of the D1 transition. With our experimental setup we can access a wide parameter range, in which the system can be characterized. By using separate light paths for the gray molasses and the MOT, we are able to investigate the influence of different polarizations and intensities on the D1 cooling feature. This enables us to cool our Li atoms from initially $\sim 250\,\mu$K after the MOT to temperatures below $50\,\mu$K. The very robust cooling technique offers us better starting conditions for our optical dipole trap, where Li sympathetically cools K.

Kurzfassung

Im FeLiKx Experiment an der Universität Innsbruck werden stark wechselwirkende Li-K Mischungen erzeugt, in welchen ^{6}Li als der Kühlagent fungiert. Die hohe Temperatur der ^{6}Li Atome in der magneto-optischen Falle (engl. magneto-optical trap "MOT"), welche am D2-Übergang von ^{6}Li betrieben wird, limitiert die Effizienz des Kühlmediums. Um diese Limitierung zu überwinden, implementieren wir eine Kühlmethode, die "graue Molasse", auf dem D1 Übergang, welche es uns ermöglicht sub-Doppler Temperaturen zu erreichen. Bei dieser Methode resultiert der Kühleffekt aus einer Kombination des Sisyphuseffekts und eines scharfen Kühleffekts nahe des Raman Überganges, der erreicht wird indem die zwei Grundzustände ($F = 1/2$ and $F = 3/2$) mittels zweier Laser, welche relativ zum angeregten Zustand $F' = 3/2$ blau verstimmt sind, gekoppelt werden. Durch den hier gewählten Aufbau der grauen Molasse erhalten wir Zugang zu einem großen Parameterbereich, mit dessen Hilfe das System charakterisiert werden kann. Die Realisierung zweier verschiedener Strahlengänge für die MOT und die Graue Molasse ermöglicht uns außerdem die Untersuchung des Einflusses verschiedener Polarisationen und Intensitäten auf den D1 Kühleffekt. Durch die Implementierung dieser zusätzlichen Kühlung von ^{6}Li sind wir in der Lage die Temperatur von ursprünglich $\sim 250\,\mu$K nach der MOT, auf weniger als $50\,\mu$K zu reduzieren. Diese sehr robuste Kühltechnik bietet uns bessere Startbedingungen für unsere optische Dipolfalle, in der Li das K sympathetisch kühlt.

Contents

Chapter 1

Introduction

In 1975 T. Hänsch and A. Schawlow proposed a method to cool an atomic vapor by laser light [1]. During the 1980's physicists slowed down an atomic beam [2], cooled the atoms with optical molasses [3], and captured them in a magneto-optical trap [4].[1] These laser cooling techniques relied on the radiation pressure an atom feels when it is exposed to laser light. A temperature limit (Doppler limit), arising from the balance between the laser cooling and heating processes, including shot noise of the laser and the random recoil of the atoms due to spontaneous emission, was predicted [7]. Around 1997, a group led by Bill Phillips developed new techniques to determine the temperature of the atoms. There they found that the atoms had temperatures below the Doppler limit. At this point new theories had to be found to explain this phenomenon. It was then seen that there are many cooling processes that can occur for certain laser configurations, which lead to sub-Doppler temperatures.

The development of laser systems and cooling methods enabled the generation of quantum-degenerate gases. The quantum-degenerate regime is reached if the inter-particle distance of an atomic cloud approaches the thermal de Broglie wavelength of the atoms. In this regime, the intrinsic properties of the atoms determine the properties of the cloud. Fermions obey the Pauli exclusion principle and therefore they follow the Fermi-Dirac statistics, while bosons behave according to the Bose-Einstein distribution.

The FeLiKx experiment at the Institute for Quantum Optics and Quantum Information (IQOQI) [8] cools the fermionic atoms, ^{6}Li and ^{40}K, in order to investigate their interactions in the quantum-degenerate regime [9, 10]. The ultracold fermions are produced by cooling and confining the Li and K atoms in magneto-optical traps and then sympathetically cooling the K atoms while evaporating Li in an optical dipole trap.

Currently, the temperature of the Li and K atoms in the FeLiKx experiment after the magneto-optical trap is close to the Doppler limit. We capture about 10^8 lithium and 10^6 potassium atoms in the magneto-optical traps. We implement a gray-molasses cooling scheme, where three counterpropagating bichromatic laser beams, consisting of a repumper and a cooler, form a standing wave. Recently, sub-Doppler cooling was demonstrated in ^{6}Li on the D1 transition by [11, 12].

In this thesis, we implement the cooling scheme after the magneto-optical trap to cool the lithium atoms to sub-Doppler temperatures. We are able to cool a fraction of about $\sim 98\,\%$ of the atoms, captured in the magneto-optical trap, from $\sim 230\,\mu$K to $\sim 40\,\mu$K. We can increase the phase-space density of our lithium cloud by a factor of 15. Therefore, we can improve the starting conditions for evaporative cooling.

The improved phase-space density at the start of evaporative cooling should lead to lower

[1] It should be noted that the first laser cooling was performed on ions [5, 6].

temperatures and higher phase-space densities in fermionic mixtures of Li and K. This would allow access to new physics of strongly interacting quantum systems. In general, the temperatures of dilute atomic clouds can be referred to their mean kinetic energy. If a sample of ultracold atoms is produced, their mean kinetic energy is low, and the short range interactions are fully described by the scattering length. In the quantum-degenerate regime, Feshbach resonances can be used to trigger the interactions between the atoms by manipulating the scattering length by the use of magnetic fields [13]. Investigations, such as atom dimer interactions [9], decoherence of impurities in a fermi sea [14] or few body physics [15], led to a better understanding of ultracold atoms. Such measurements rely on controllable systems with well known loss channels. Finite temperatures can lead to decoherence of an atomic sample and therefore the procedure of cooling a high fraction of captured atoms by laser cooling can be an important step to investigate deeply-degenerate Fermi gases. In the FeLiKx experiment, further lowering the temperature of lithium can lead to new physics of impurities in a Fermi sea [16]. An improved cooling of both, potassium and lithium, could lead to new exotic phases [17–19]

Chapter 2

Introduction to Laser Cooling

Laser cooling is a method to achieve low temperatures in dilute atomic clouds, by emission and absorption of photons. Depending on the atomic species, temperatures below $1\,\mathrm{mK}$, and sometimes even below $1\,\mu\mathrm{K}$, can be reached. In this chapter the derivation of the scattering force in a two-level atom is introduced. With this the term "optical molasses" can be explained and the Doppler limit can be derived. The last section treats the phase-space density, a quantity that is also important in ultracold physics. It compares the inter-particle distance and the thermal de Broglie wavelength, and therefore states whether quantum statistical effects become important in a dilute atomic cloud.

2.1 Scattering Force

A two-level atom consists of a ground state $|g\rangle$ and an excited state $|e\rangle$ with energy splitting $\Delta E_0 = \hbar\omega_0 = h\nu_0$, where h denotes the Planck constant and ν_0 is the atom's transition frequency. The atom is placed in a resonant laser field with angular frequency $\omega_\mathrm{L} \approx \omega_0$ propagating along the x-axis. The atom moves along the same axis with a velocity v and therefore it "sees" a different frequency due to the Doppler effect, as illustrated in Figure 2.1. If the atom moves towards the light source it experiences a higher frequency $\omega_\mathrm{L} + k_\mathrm{L} v$, with k_L being the wavenumber of the light. In the opposite case, where the atom moves away from the laser source, it sees a smaller frequency.

The deviation of the laser from resonance is called the detuning $\Delta = \omega_L - \omega_0$. To account for the Doppler effect, the frequency has to be corrected by $k_\mathrm{L} v$. If the difference of the Doppler shifted frequency of the laser beam is higher (smaller) than the atoms transition frequency, the light is said to be blue (red) detuned. With the inclusion of the Doppler effect, the scattering force acting on an atom can now be derived by using equation (A.19) derived in the Appendix A.1. The excited state population

$$\rho_{22} = \frac{\Omega^2/4}{(\Delta + k_\mathrm{L} v)^2 + \Omega^2/2 + \Gamma^2/4}$$

can be described in dependence of the Rabi frequency Ω and the natural decay rate Γ of the excited state. If an atom absorbs a photon, the photon momentum $\hbar k_\mathrm{L}$ is transferred to the atom. Therefore, the acting force is described by the photon momentum times the scattering rate $R_\mathrm{sc} = \Gamma\rho_{22}$. Due to the Doppler effect, the scattering force

$$F_\mathrm{sc} = \hbar k_\mathrm{L} \times \Gamma\rho_{22} = \hbar k_\mathrm{L} \frac{\Gamma}{2} \frac{\Omega^2/2}{(\Delta + k_\mathrm{L} v)^2 + \Omega^2/2 + \Gamma^2/4} \tag{2.1}$$

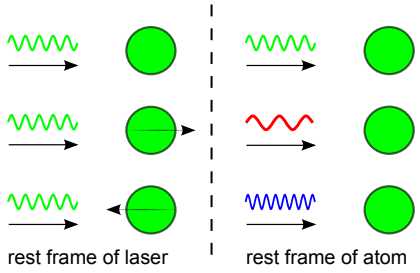

Figure 2.1. Illustration of the Doppler effect. In the rest frame of the light source, the atom stands still (top), moves in the direction of the radiation field (middle), and moves against it (bottom). The change to the atoms rest frame illustrates how the atom 'sees' different wavelengths.

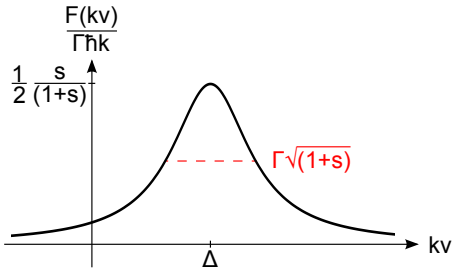

Figure 2.2. Scattering force dependent on the Doppler shift $k_{\mathrm{L}}v$ for a fixed detuning Δ. The force is depicted in units of $\Gamma\hbar k_{\mathrm{L}}$. The full width at half maximum is marked red.

is a velocity dependent force. After introducing the saturation intensity $I_{\mathrm{sat}} = (\pi/3) \times (hc\Gamma/\lambda^3)$ and its relation to the Rabi frequency $\Omega^2 = (I/I_{\mathrm{sat}}) \times (\Gamma^2/2)$ [20], the scattering force can be rewritten into the compact form

$$F_{\mathrm{sc}} = \hbar k_L \frac{\Gamma}{2} \frac{I/I_{\mathrm{sat}}}{1 + I/I_{\mathrm{sat}} + 4(\Delta + k_{\mathrm{L}}v)^2/\Gamma^2}, \tag{2.2}$$

which is illustrated in Figure 2.2. The maximum of this force arises when the detuning compensates for the Doppler shift $\Delta = k_{\mathrm{L}}v$. An atom's velocity is increased (decreased) if it moves in the direction (opposite direction) of the propagation direction of the laser beam. The saturation parameter $s = I/I_{\mathrm{sat}}$ and the linewidth determine the strength of the scattering force, as well as the full width at half maximum (FWHM).

This velocity dependent scattering force can be used to slow down an atomic beam, for instance starting from an oven, by a laser beam coming from the opposite direction. The ^{6}Li atom has a scattering rate of about 10^7 photons per second in the presence of a resonant laser field. The resulting force leads then to an acceleration of the atom that is about 5×10^4 times stronger than the gravitational acceleration g. As the atom travels over a distance of $d = 10\,\mathrm{cm}$ with an initial speed of $500\,\mathrm{m/s}$ the frequency of the laser, in the rest frame of the atom, changes by an amount of $\sim 1\,\mathrm{GHz}$, due to the Doppler effect. At this point, the acceleration is significantly reduced by two orders in magnitude. Thus, if an atomic beam needs to be efficiently slowed down the Doppler effect must be compensated for.

2.2 Optical Molasses

To explain an optical molasses, a dilute cloud of atoms with low velocities $kv \lesssim \Gamma$ is considered, where every atom is able to move in all directions. Therefore, to lower their temperature, two beams are positioned vis-à-vis from each other in all three dimensions, such that the intersection of these six beams overlaps with the position of the atoms. This setup is illustrated in Figure

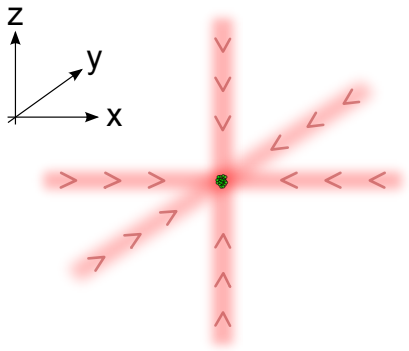

Figure 2.3. Atoms in optical molasses. Three counter propagating beams cover the three dimensions. The atoms (green) are located at their intersection.

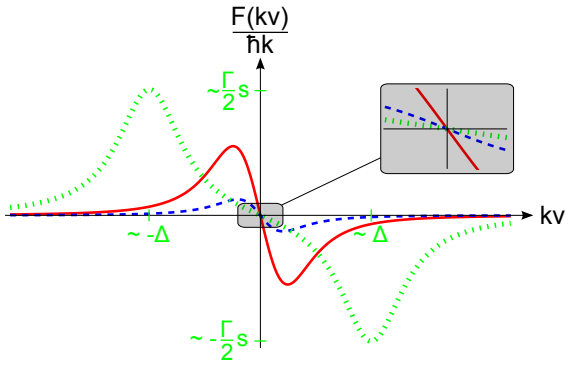

Figure 2.4. Molasses Force dependent on the Doppler shift for different detunings. The red line corresponds to a detuning of $\Delta = -\Gamma/2$, the blue dashed line to $\Delta = -\Gamma/10$, and the green dotted line to $\Delta = -3\Gamma$. The gray shaded region is a zoom of the low velocity regime.

2.3. A naive assumption for what happens to the atoms would be that the force arising from one beam will be canceled out by the force arising from the counterpropagating beam. This is in fact true for atoms at rest; however, for atoms with non-zero velocity, the Doppler effect leads to an imbalance in the forces. The atoms will absorb more light from the laser beam they are traveling to than from the counterpropagating one.

For further calculations it shall be assumed that the intensity of the beams is lower than the saturation intensity $s \ll 1$, and hence stimulated emission can be neglected. For simplicity of calculating the molasses force F_{mol} only one direction with two counterpropagating beams will be considered now:

$$F_{\text{mol}} = F_{\text{sc}}(\Delta - kv) - F_{\text{sc}}(\Delta + kv) \tag{2.3}$$

$$\approx 4\hbar k^2 s \frac{2\Delta v/\Gamma}{(1 + 4(\Delta - kv)^2/\Gamma^2)(1 + 4(\Delta + kv)^2/\Gamma^2)} \tag{2.4}$$

Figure 2.4 illustrates the force on the atoms in the molasses calculated in equation (2.4) for three different detunings $\Delta = -\Gamma/10, -\Gamma/2, -3\Gamma$. The maximum and minimum of the molasses force at a large detuning $\Delta = -3\Gamma$ is approximately equal to the case where only one laser beam is present. For a smaller detuning the deviations get bigger. In case of a negative (i.e. red) detuning the resulting force is negative for $v > 0$, and positive for $v < 0$ which results in a deceleration of the atoms. In the low velocity regime $k_{\text{L}} v \ll \Gamma$, the molasses force can be approximated to

$$F_{\text{mol}} \approx 4\hbar k^2 s \frac{2\Delta/\Gamma}{(1 + (2\Delta/\Gamma)^2)^2} \times v \tag{2.5}$$

by a linear Taylor expansion of $k_{\text{L}} v/\Gamma$ around zero. In this regime, which is illustrated as the gray shaded area in Figure 2.4, the force is proportional to the velocity. If compared to the

friction force acting on a particle in a viscous medium, the atoms in such a light field can be seen to move as in a treacle or molasses with a friction coefficient

$$\alpha = -4\hbar k^2 s \frac{2\Delta/\Gamma}{(1+(2\Delta/\Gamma)^2)^2}, \tag{2.6}$$

which reduces the molasses force to $F_{\text{mol}} = -\alpha v$ - hence the term *optical molasses*.

It shall be noted that it is crucial in an experiment to choose the right sign of the detuning. If the laser is blue detuned the molasses force would be maximal for positive and minimal for negative velocities. The result is heating of the atoms.

2.3 Doppler Limit

In an atomic cloud arranged in a radiation field, not only cooling but also heating processes occur. The equilibrium temperature is reached, when the cooling power is as large as the heating power.

An atom in its excited state spontaneously emits a photon with the same probability into one direction as into the opposite. This implies that the mean momentum transfer of spontaneous emission is equal to zero. Due to the randomness of the process of spontaneous emission the atom's momentum undergoes a random walk and therefore the mean squared momentum $\langle p_{\text{sp}}^2 \rangle$, which is proportional to the mean kinetic energy $\langle E_{\text{sp}} \rangle$, has a non-zero value [20]. During a time interval of duration t, with every emission process the atom is kicked into a random direction at a rate R_{sc} with the strength of the recoil momentum $p_{\text{r}} = \hbar k_{\text{L}}$ which manifests itself in heating the atom. The resulting mean kinetic energy is then

$$\langle E_{\text{sp}} \rangle = \frac{\langle p_{\text{sp}}^2 \rangle}{2M} = \frac{p_{\text{r}}^2}{2M} R_{\text{sc}} t. \tag{2.7}$$

Another heating effect results from the photons spatial distribution. Under the simplified assumption of a Poissonian distribution the number of absorbed photons per time fluctuates by $\sqrt{\overline{N}}$ around the mean value $\overline{N}$. Subsequently, the mean kinetic energy induced by this process is

$$\langle E_{\text{abs}} \rangle = \frac{p_{\text{r}}^2}{2M} R_{\text{sc}} t. \tag{2.8}$$

Now that the heating effects are discovered, with a little help from Newton, and the molasses force, the cooling and heating powers in steady state can be determined

$$\left\langle \frac{d}{dt}\left(\frac{p^2}{M}\right) \right\rangle = \left\langle \frac{p}{M}\frac{dp}{dt} \right\rangle = \left\langle \frac{p}{M} F_{\text{mol}} \right\rangle = -\frac{\langle p^2 \rangle}{M^2}\alpha \tag{2.9}$$

$$\left\langle \frac{d}{dt}(E_{\text{sp}} + E_{\text{abs}}) \right\rangle = \frac{p_{\text{r}}^2}{M} R_{\text{sc}}. \tag{2.10}$$

Equation (2.9) shows the cooling, and equation (2.10) the heating processes in an atomic cloud. The lowest temperature will be achieved when the two processes are equal in strength, i.e.

$$\frac{\langle p^2 \rangle}{M^2}\alpha = \frac{p_{\text{r}}^2}{M} R_{\text{sc}}. \tag{2.11}$$

The coefficient α, defined in equation (2.6), can be inserted and the equation can then be rewritten to

$$\frac{\langle p^2 \rangle}{M} = \frac{\hbar\Gamma}{8} \frac{1 + (2\Delta/\Gamma)^2}{-2\Delta/\Gamma}. \tag{2.12}$$

With the aid of the equipartition theorem, which states that in one dimension $\langle p^2 \rangle / M = k_\mathrm{B} T$ with k_B being the Boltzmann constant, the temperature

$$T = \frac{\hbar\Gamma}{8k_\mathrm{B}} \frac{1 + (2\Delta/\Gamma)^2}{-2\Delta/\Gamma} \tag{2.13}$$

can be found. The first derivative of the temperature unveils the minimum at a detuning of $\Delta = -\Gamma/2$. At this detuning the Doppler limit

$$T_\mathrm{D} = \frac{\hbar\Gamma}{2k_\mathrm{B}} \tag{2.14}$$

can be reached. This limit can now be calculated for every atomic species. In case of ^{6}Li, the linewidth is $\Gamma = 2\pi \times 5.87\,\mathrm{MHz}$ and therefore the Doppler temperature amounts to approximately $140\,\mu\mathrm{K}$.

Until the 1980's, physicists expected the Doppler temperature to be the lowest by laser cooling achievable temperature. Nowadays, lower temperatures can be achieved, by so-called sub-Doppler cooling techniques. Laser cooling with the mechanism described above is referred to as *Doppler cooling* and limited by the Doppler temperature.

2.4 Phase-Space Density

In kinetic theory, atoms reach a thermal equilibrium with the walls of the repository they are in by collisions. The atoms, of mass M, and the walls have the same temperature after thermalization. The mean kinetic energy of the atoms corresponds to the temperature T of the ensemble. From this it follows that if the walls of the repository get cooled, the atoms mean kinetic energy is reduced by heat transfer and the temperature decreases.

The velocities in a thermal atomic cloud follow the Maxwell-Boltzmann distribution [21]. By calculating the root mean square velocity $v_\mathrm{rms} = \sqrt{v_\mathrm{x}^2 + v_\mathrm{y}^2 + v_\mathrm{z}^2}$, the relation to temperature

$$\frac{1}{2} M v_\mathrm{rms}^2 = \frac{3}{2} k_\mathrm{B} T \tag{2.15}$$

is found (equipartition theorem). Atoms that get laser cooled do not interact with a reservoir but rather with a light field. The mean kinetic energy can be changed when the atoms interact with the light field.

The wave character of an atom is described by the de Broglie wavelength $\lambda_\mathrm{dB} = h/p$, where p is the atomic momentum. In this picture the atom is fully delocalized. The *thermal* de Broglie wavelength λ_th is approximately described by the mean de Broglie wavelength at a certain temperature T of non-relativistic atoms in an ideal gas. It can be interpreted as the uncertainty to find a particle at a certain position in space [20]. As the temperature - and

therefore the velocity - decreases, the uncertainty grows. Equation (2.15) leads then to an expression of $\lambda_{\text{th}} = h/(\sqrt{3k_{\text{B}}TM})$. This is one of the conventions to express the thermal de Broglie wavelength. The second one - used in this thesis - arises from the calculation of the partition function, which is used to derive several thermodynamic quantities. In this derivation, a characteristic length scale arises

$$\lambda_{\text{th}} = \frac{h}{\sqrt{2\pi k_{\text{B}}TM}} \tag{2.16}$$

that describes the spatial extend of a particle. This quantity is often used as a connector between classical and quantum mechanics. The dimensionless phase-space density

$$\rho_{\text{psd}} = n \times \lambda_{\text{th}}^3 = \frac{N}{V} \times \left(\frac{h}{\sqrt{2\pi k_{\text{B}}TM}}\right)^3 \tag{2.17}$$

results from a comparison of the particle density $n = N/V$ and λ_{th}. The cube root of the volume divided by the atom number, $(V/N)^{1/3}$, corresponds to the inter-particle distance. As the definition of λ_{th} is given by equation (2.16), the phase-space density gives the probability of particles to be - in phase space - in a box of size $\hbar^3$ [22]. If the thermal de Broglie wavelength approaches the inter-particle distance, the wavefunctions overlap, and quantum-statistical effects become important ($\rho_{\text{psd}} \approx 1$).

Values observed in the FeLiKx experiment at the University of Innsbruck [8] show that after standard Doppler cooling, about 10^8 ^{6}Li atoms are brought to a temperature of $\sim 250\,\mu$K. With a cloud volume of approximately $4\,\text{mm}^3$, the phase-space density amounts to $\rho_{\text{psd}} \approx 7 \times 10^{-6}$. This value can then be improved to reach quantum degeneracy through another cooling stage called evaporative cooling [23] where the gain in phase-space density is accompanied by particle loss. The starting conditions for such an additional cooling stage can be improved (lower T at roughly same N) through a sub-Doppler cooling technique. If the temperature is decreased by roughly a factor of five at equal atom number and volume of the cloud, ρ_{psd} increases by one order of magnitude. This increase can also be achieved by evaporative cooling though, as mentioned before, it goes side by side with a particle loss. One would have to sacrifice a factor of two to three in atom number to improve ρ_{psd} by a factor of ten.

To summarize, the scattering force results from absorption of photons and energy that gets dissipated through the process of spontaneous emission. An atomic beam can be slowed down significantly over a small distance provided that the Doppler effect can be compensated. These atoms can be captured in atom traps, where optical molasses can be used to further reduce the atoms' temperature. The temperature limit that can be reached if the atom is considered to be a two-level atom is called the Doppler limit and is derived by comparing the heating and cooling effects in optical molasses. The fact that in laser cooling a dissipative force is acting on the atoms leads to the ability of increasing the phase-space density of a dilute atomic cloud, which is important if quantum degeneracy is required.

Chapter 3

Beyond the Two-Level Atom

To understand the principles of different sub-Doppler cooling techniques, it is not sufficient to treat an atom as a two-level object. The different cooling processes in optical molasses can be described by considering the variety of energy levels in atoms. Furthermore, the light has to be treated in more detail, as the orientation of the electric field with respect to the atom, and the light induced shifts of atomic energy levels play a crucial role in sub-Doppler cooling. Therefore, this chapter will go beyond the two-level atom picture and introduce some properties of light and atoms and their interaction.

3.1 Multi-level Atoms

It is convenient to introduce the basics of Doppler-limited laser cooling using a simple two-level system to represent the atom. For the sake of understanding sub-Doppler cooling however, it is necessary to consider that light can excite an electron to more than one level in an atom. This section gives an overview over the origin of the energy levels, illustrated in 3.1 in case of a ^{6}Li atom. The explanations are based on the textbook *Quantum Physics of Atoms, Molecules, Solids, Nuclei and Particles* by Robert Eisberg and Robert Resnick [24] in which more detailed calculations can be found.

The measurable structure of atoms is expressed by the quantum numbers. In a two-level configuration it is sufficient to describe the atom by:

- The *principal quantum number* n describes the energy level in which the electron is located. It can only take integer values ($n = 1, 2, 3, ...$).
- The orbital angular momentum $\mathbf{l}$ of the electron is described by the *angular quantum number* l. It can take on the n integer values: $l = 0, 1, ..., n - 1$. Often another notation is used: $l = s, p, d, ...$
- The *magnetic quantum number* m_l determines the projection of the angular momentum on the z-axis. The $2l + 1$ values it can take reach from $-l$ to l

In Figure 3.1 it can be seen that, for a two-level, atom the ground and excited states are described by n and l.

The consideration of the electron's spin gives rise to the *fine structure*. In the rest frame of the electron, the nucleus can be considered to orbit around it. This moving charge (current) induces a magnetic field at the position of the electron. The electron possesses a magnetic dipole moment due to its spin $\mathbf{s}$. This dipole tends to align itself either parallel or anti-parallel to the

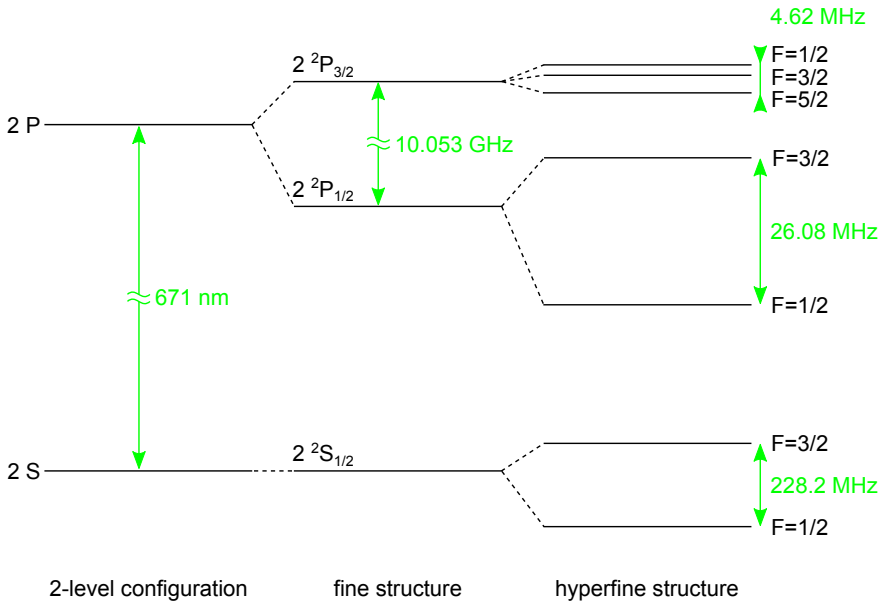

Figure 3.1. Energy levels of ^{6}Li. The ground 2S ($n = 2$, $l = 0$) and excited 2P ($n = 2$, $l = 1$) states are shown. The spectroscopic notation $n^{2s+1}l_j$ is used to describe the fine structure energy levels. Values taken from [8].

magnetic field, giving rise to different potential energies depending on the spin's orientation. Therefore, the *spin-orbit coupling* results in a splitting of the energy levels, dependent on l and s (spin quantum number), giving rise to the fine structure. The spin and the orbital angular momentum can be summed up to the *total angular momentum of the electron* $\mathbf{j} = \mathbf{l} + \mathbf{s}$. Figure 3.1 illustrates the fine structure of a ^{6}Li atom. The energy levels are described by an additional integer quantum number j, which has $2j + 1$ projections m_j, with $|l - s| \leq j \leq |l + s|$ and $-j \leq m_j \leq j$.

The protons and neutrons, which build up the nucleus of the atom, also possess a spin. Due to that, the nucleus has a nuclear magnetic moment **I** - with quantum number I - that couples to the total angular momentum of the electron **j** in a similar manner as the spin-orbit coupling and gives rise to the *total angular momentum of the atom* **F = j + I**. The quantum number F can take values from $|I - j|$ to $|I + j|$ in integer steps. This results in another splitting of the fine structure levels, namely the *hyperfine splitting* of the energy levels, shown in Figure 3.1.

3.2 Polarization

Light - propagating in an isotropic medium, and in free space - is described as a transverse wave, which means that the electric and magnetic fields oscillate in a plane perpendicular to the propagation direction. For further explanations it shall be considered that a monochromatic wave with angular frequency $\omega_\mathrm{L} = 2\pi\nu_\mathrm{L}$ is propagating along the z-axis in free space at speed

c. The electric field, oscillating in the $x-y$ plane, can be described by the equations [25]

$$E_{\mathrm{x}}(z,t) = E_{0,\mathrm{x}}\,\mathrm{Re}(e^{i(\omega_{\mathrm{L}}(z/c-t)+\phi_{\mathrm{x}})}), \tag{3.1}$$

$$E_{\mathrm{y}}(z,t) = E_{0,\mathrm{y}}\,\mathrm{Re}(e^{i(\omega_{\mathrm{L}}(z/c-t)+\phi_{\mathrm{y}})}), \text{ and} \tag{3.2}$$

$$E_{\mathrm{z}}(z,t) = 0. \tag{3.3}$$

The phase $\phi = \phi_{\mathrm{x}} - \phi_{\mathrm{y}}$ and the amplitudes $E_{0,\mathrm{x}}$, $E_{0,\mathrm{y}} \in \mathbb{R}$ state the type of polarization, as can be seen in Figure 3.2. Equations (3.1) and (3.2) satisfy the parametric representation of an ellipse. As the beam propagates along the z axis, the electric-field vector $\mathbf{E}(z,t)$ undergoes the path of an elliptical helix in the $x-y$ plane. At certain amplitude and phase values, the ellipse turns into a circle or a line. These two limiting cases of elliptical polarization are:

- linear polarization: $\phi = 0, \pi$ with $\hat{\mathbf{e}}_{\mathrm{pol}} = (a\hat{\mathbf{e}}_{\mathrm{x}} + b\hat{\mathbf{e}}_{\mathrm{y}})/\sqrt{a^2+b^2}$ and $a, b \in \mathbb{R}$
- circular polarization: $\phi = \pm\pi/2$ and $E_{0,\mathrm{x}} = E_{0,\mathrm{y}}$ with $\hat{\mathbf{e}}_{\mathrm{pol}} = (\hat{\mathbf{e}}_{\mathrm{x}} \pm i\hat{\mathbf{e}}_{\mathrm{y}})/\sqrt{2}$

The unit polarization vector, $\hat{\mathbf{e}}_{\mathrm{pol}}$, describes the polarization using the unit vectors $\hat{\mathbf{e}}_{\mathrm{x}}$ and $\hat{\mathbf{e}}_{\mathrm{y}}$ along the x- and y-axis, respectively. If the unit polarization vector is $(\hat{\mathbf{e}}_{\mathrm{x}} - i\hat{\mathbf{e}}_{\mathrm{y}})/\sqrt{2}$ the electric field oscillating in the y-direction lags in phase with respect to the x-direction by $\pi/2$. The resulting total electric field is circularly polarized. This means that in this representation, a factor of i corresponds to a phase shift of $\pi/2$. It should be noted that the circular polarization can either be left or right handed. If the thumb of the right (left) hand points towards the propagation direction of the laser beam and the rest of the fingers follow the rotation direction of the electric field the light is called right (left) handed.

The handiness of the polarization of a laser beam is defined without a reference to a particular quantization axis $\hat{\mathbf{e}}_{\mathrm{q}}$. However in an experiment it is convenient to know the polarization of the light with respect to the atom. Therefore, a magnetic field can be applied along the z-direction $\mathbf{B} = (0, 0, B_{\mathrm{z}})$, which is chosen to be the quantization axis. If one speaks of polarizations with respect to such a quantization axis the terms π, σ^+ and σ^- are used. If the electric field of a linearly polarized laser beam is parallel to $\hat{\mathbf{e}}_{\mathrm{q}}$ it has π-polarization with respect to the quantization axis. On the other hand, if the light is left-handed (right-handed) circularly polarized and propagates along $\hat{\mathbf{e}}_{\mathrm{q}}$ it is said to be σ^--polarized (σ^+-polarized).

3.3 Selection Rules

If the oscillation frequency of the electric field of a laser beam matches the energy difference $E_{|2\rangle} - E_{|1\rangle} = \hbar\omega_{\mathrm{L}}$ of two electronic states of the atom $|1\rangle$ and $|2\rangle$, the atom is turned into a superposition of these two states and an oscillating electric dipole moment $\mathbf{p} = \alpha\mathbf{E}(t)$ is induced. In contrast to the previous chapter, in this section α denotes the polarizability of the atom. It states the ability of a charge distribution, e.g. electrons in an atom, to be distorted from their positions due to the presence of an electric field $\mathbf{E}(t) = E_0\,\mathrm{Re}(e^{-i\omega_{\mathrm{L}}t}\hat{\mathbf{e}}_{\mathrm{pol}})$.[2] The oscillating electric field of a laser beam can be interpreted as a photon flux. Each photon carries

[2] In contrast to equations (3.1) and (3.2) the exponent does not depend on the position. The dipole approximation, which assumes that the wavelength of the light is much larger than the size of the atom, is applied.

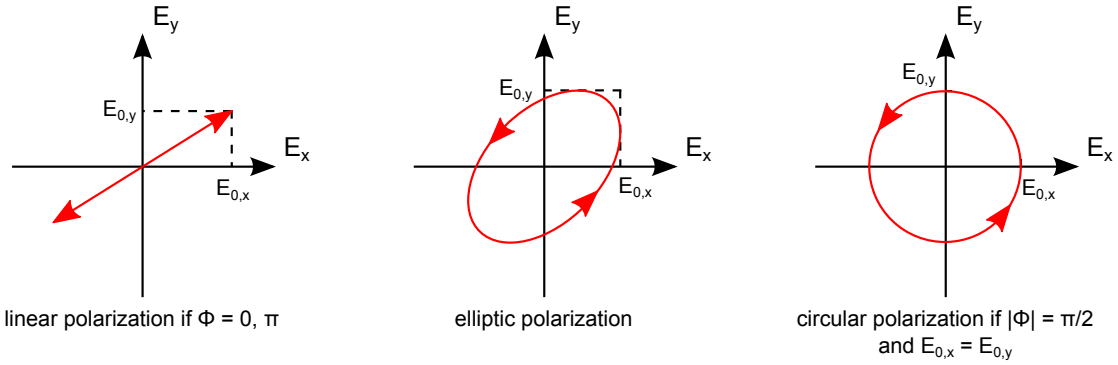

Figure 3.2. Different polarizations for a fixed value of z. The arrows mark the direction of the oscillating electric-field vector in time.

angular momentum. If an atom undergoes a transition from one to another state by absorbing a photon, angular momentum conservation must be fulfilled. Therefore, the kind of transition that is allowed depends on the polarization of the light field and so-called *selection rules* can be formulated.

Photons are spin-1 particles and therefore bosons. The helicity of circularly polarized photons equals $\pm\hbar$ and we can define a quantum number j_p and its projections on the quantization axis m_{j_p} analogous to the atomic quantum numbers j and m_j. If an atom absorbs a photon, angular momentum conservation must be fulfilled and the final angular momentum of the atom is $\mathbf{j'} = \mathbf{j}_p + \mathbf{j}$. From this consideration one can see:

- For π-polarization the photon's momentum with respect to the quantization axis is $j_p = 0$, hence $\Delta j = 0$.
- For $\sigma^{\pm}$-polarization the photon's momentum with respect to the quantization axis is $j_p = \pm 1$, hence $\Delta j = \pm 1$

Thus, if an atom absorbs a photon the atomic angular momentum changes by the corresponding value. Table 3.1 summarizes the dipole-allowed transitions for the above mentioned relative polarizations of the light. The excited levels are marked by an apostrophe. For the transition

dipole-allowed transitions	restriction
$\Delta s = 0$	
$\Delta l = \pm 1$	
$\Delta m_l = 0, \pm 1$	$\pi, \sigma^{\pm}$ polarization
$\Delta j = 0, \pm 1$	not $j = 0$ to $j' = 0$
$\Delta m_j = 0, \pm 1$	$\pi, \sigma^{\pm}$ polarization
$\Delta F = 0, \pm 1$	not $F = 0$ to $F' = 0$
$\Delta m_F = 0, \pm 1$	$\pi, \sigma^{\pm}$ polarization

Table 3.1. Selection rules for dipole transitions [20].

$\Delta l = 0$ one has to consider not only the conservation of angular momentum but also the conservation of parity in such a process [26].

3.4 Dipole Force and Light Shift

In the previous chapter, the scattering force F_{sc} was introduced. Another force that arises from the atom light interaction is called the dipole, or gradient force F_{dip}. It arises from the refraction of light at an object with a different refractive index than its surrounding. Light quanta carry momentum, and as soon as they get refracted, a part of their momentum is transferred to the object while momentum conservation is fulfilled. If a refractive object is placed in a focused laser beam, it will be drawn into the region of maximum (minimum) intensity if its refractive index is greater (smaller) than the one of the surrounding.

The dipole force is a conservative force. Therefore, the force $\mathbf{F}_{\text{dip}} = -\nabla U$ can be derived from a potential U. In this potential atoms can be trapped[3], but there is no cooling mechanism directly related to $\mathbf{F}_{\text{dip}}$. The dipole force in one dimension is derived in the appendix (A.2) and takes the form

$$\mathbf{F}_{\text{dip}} = -\frac{\hbar\Delta}{2}\frac{\Omega}{\Delta^2 + \Omega^2/2 + \Gamma^2/4}\nabla\Omega. \tag{3.4}$$

If the laser is resonant to the transition of the atom, i.e. $\Delta = 0$, the dipole force vanishes. Another interesting case is if the light if far detuned $|\Delta| \gg \Gamma$ and the intensity is such that $|\Delta| \gg \Omega$. Then

$$\mathbf{F}_{\text{dip}} \approx -\nabla\left(\frac{\hbar\Omega^2}{4\Delta}\right) \tag{3.5}$$

and the potential is $U = \hbar\Omega^2/(4\Delta)$. The change in the potential energy of the atom due to the light is called the *light shift*.

The calculation for this energy shift is straight forward. Starting from the differential equation of the population coefficients $\tilde{c}_1$ and $\tilde{c}_2$ derived in (A.12),

$$i\frac{\mathrm{d}}{\mathrm{d}t}\begin{pmatrix}\tilde{c}_1\\ \tilde{c}_2\end{pmatrix} = \frac{1}{2}\begin{pmatrix}\Delta & \Omega\\ \Omega & -\Delta\end{pmatrix}\begin{pmatrix}\tilde{c}_1\\ \tilde{c}_2\end{pmatrix} \tag{3.6}$$

the eigenvalues, corresponding to the energy shift, are $\lambda = \pm\sqrt{\Delta^2 + \Omega^2}/2$. It shall be noted that the matrix described in equation (3.6) corresponds to the interaction Hamiltonian and the two eigenvalue differ by the so-called generalized Rabi frequency

$$\tilde{\Omega} = \sqrt{\Delta^2 + \Omega^2}. \tag{3.7}$$

For the case of a large detuning $\Delta \gg \Omega$ the eigenvalues can be approximated to $\lambda \approx \pm(\Delta/2 + \Omega^2/(4\Delta))$. This result can be understood as two states being separated by Δ, and "feeling" a light shift of $\delta = \pm\hbar\Omega^2/(4\Delta)$.

3.5 Dressed-Atom Model

Besides the optical Bloch equations the atom-light interaction can also be described by the dressed-atom model. In this approach, the laser field is treated quantum mechanically, which

[3] Many experiments working with ultracold atoms make use of the so-called dipole traps exploiting the dipole force [27].

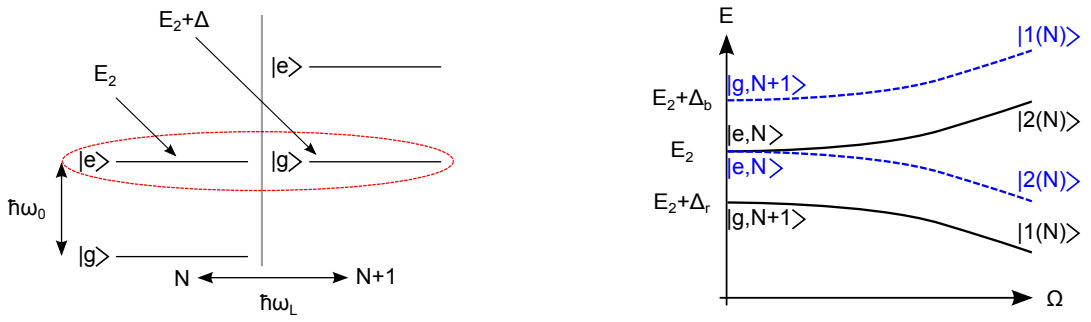

Figure 3.3. Illustration of the Stark shift. Panel (a) depicts the ground $|g\rangle$ and excited $|e\rangle$ states of an atom in the presence of N and $N+1$ photons in the laser field, respectively. In panel (b) a zoom of the red dashed encircled states of (a) for various coupling strengths Ω is shown. The black solid (blue dashed) line indicates the level shift for a negative (positive) detuning Δ_r (Δ_b) of the laser frequency ω_L with respect to the atomic transition frequency ω_0.

gives more insight into the processes of spontaneous emission, stimulated emission and absorption of a photon by an atom.

The total Hamiltonian $\mathcal{H} = \mathcal{H}_\mathrm{A} + \mathcal{H}_\mathrm{L} + \mathcal{H}'$ that describes the atom in a light field consists of the sum of the atom Hamiltonian $\mathcal{H}_\mathrm{A}$, the light Hamiltonian $\mathcal{H}_\mathrm{L}$, and their interaction $\mathcal{H}'$. The eigenstates of this system consist of information about the atomic state and the laser field. The atoms can be interpreted as being dressed by the light and therefore this model is called the *dressed-atom model*.

For now, the interaction shall be switched off $\mathcal{H}' = 0$. Figure 3.3 (a) illustrates the atomic ground and excited state. The cases where N and $N+1$ photons with energy $\hbar\omega_\mathrm{L}$ are present in the laser field represent two bunched manifolds of the systems eigenstates. The energy of the eigenstates $|e, N\rangle$ (atom in excited state, N photons) and $|g, N+1\rangle$ (atom in ground state, $N+1$ photons) are separated by the detuning $\Delta = \omega_\mathrm{L} - \omega_0$. These states are shown in Figure 3.3 (a) in the red dashed encircled area and as a zoom in Figure 3.3 (b) at $\Omega = 0$. The energy shift of the state $|g, N+1\rangle$ is positive (negative) for blue (red) detuning $\Delta_\mathrm{b} > 0$ ($\Delta_\mathrm{r} < 0$).

Now, the interaction shall be turned on, $\mathcal{H}' \neq 0$. Figure 3.3 (b) illustrates the shift in energy of the perturbed system, as calculated in the last section, for different signs of the detuning. The corresponding new eigenstates

$$|1, (N)\rangle = A(\Omega, \Delta)\,|e, N\rangle + B(\Omega, \Delta)\,|g, N+1\rangle \tag{3.8}$$
$$|2, (N)\rangle = C(\Omega, \Delta)\,|e, N\rangle + D(\Omega, \Delta)\,|g, N+1\rangle \tag{3.9}$$

are a superposition of the eigenstates of the unperturbed system, where A, B, C and D denote coefficients dependent on the chosen laser intensity and detuning. It can be seen in Figure 3.3 (b) that the splitting of the dressed states gets larger as the intensities are being increased.

As mentioned before, many sub-Doppler laser-cooling techniques rely on the multi-level structure of an atom. Therefore, the Rabi-frequency $\Omega = \langle 1|e\mathbf{r}\,\mathbf{E}_0|2\rangle\,/\hbar$ (see appendix A.1) can be extended from a two-level to a multi-level picture. Considering the hyperfine structure of an atom, the eigenstates of the atom are defined by their quantum numbers n, F, and m_F, and one describes them in the basis $|nFm_\mathrm{F}\rangle$. The electric field, however directly couples to the

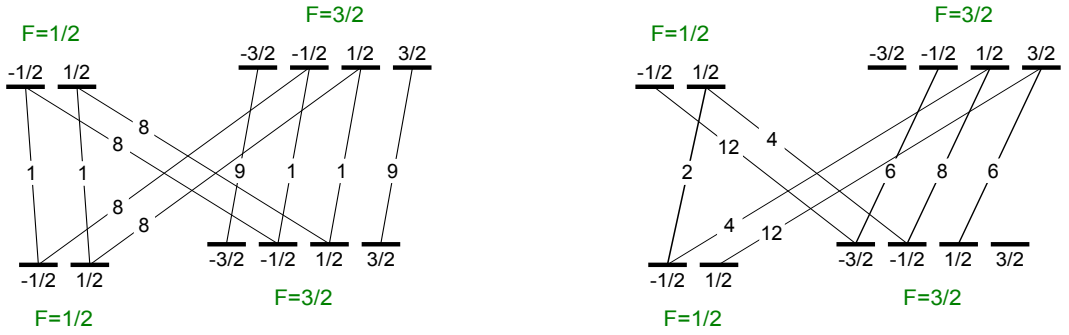

Figure 3.4. Transition strengths for a ^{6}Li atom for linear (a) and circular (b) polarization. The hyperfine states of the D1 line from $2s_{1/2}$ to $2p_{1/2}$ are illustrated. Transition strengths between different m_f states are normalized in a way that the weakest transition has an integer value [21].

orbital angular momentum **l**. It is necessary to switch the basis from $|nFm_\mathrm{F}\rangle$ to $|lm_\mathrm{l}; sm_\mathrm{s}\rangle$ to calculate the Rabi frequency or the transition rate, respectively. The proportionality factors for such basis changes are called the *Clebsch-Gordan coefficients*. They represent the overlap of different representations of the eigenstates [28]. From these coefficients the transition strengths are calculated. Figure 3.4 illustrates various sub-levels of the D1 transition in ^{6}Li from $2s_{1/2}$ to $2p_{1/2}$ and their corresponding relative transition strengths for circular and linear polarization.

To summarize this chapter, the fine and hyperfine structure of the atom was considered. Then, the basic interactions of photons with multi-level atoms were introduced. If an atom absorbs a photon, angular momentum conservation has to be fulfilled and therefore only certain transitions are dipole-allowed. This fact is described by the selection rules. Depending on the light's polarization the different energy levels can be addressed with different transition strengths, which can be determined via the Clebsch-Gordan coefficients.

The force acting on an atom in a laser beam can be separated into dissipative/scattering and non-dissipative/dipole force. The latter is conservative and therefore gives rise to a potential, which can be used to trap the atoms and shift their energy. The light shift is different for different sub-levels of the atom. In such a system it is advantageous to introduce the dressed-atom model, to obtain the energies and eigenstates of the atom-light system.

Chapter 4

Sub-Doppler Cooling

Sub-Doppler cooling (SDC) is a technique to cool atoms to temperatures below the Doppler limit. This chapter presents a sub-Doppler cooling technique where atoms are cooled by the Sisyphus effect in combination with a sub-recoil cooling method involving a dark state. This chapter shall provide a better understanding of how the gray molasses technique, which is used in this thesis to cool a cloud of fermionic 6-lithium atoms to sub-Doppler temperatures, can be interpreted.

To cool atoms to temperatures below the Doppler limit, in general they first get confined, for example, in a magneto-optical trap (MOT), where an optical molasses in combination with a quadrupole magnetic field is used to capture and cool atoms. The principles of a MOT can be found in standard textbooks such as [20, 21], and will not be treated in this thesis. It shall be noted that it is used as the starting point for sub-Doppler cooling in the experiments of this thesis.

4.1 Sisyphus Cooling

Two Sisyphus-cooling schemes, for different intensities and different signs of the detuning, are presented in this section. The particular explanations differ from each other though there is always a loss of kinetic energy of the atoms involved as it climbs a potential hill. Due to the dipole force in a standing-wave field, the atom moves in a periodic potential. As the atom moves, it climbs up a potential hill so that its kinetic energy is converted into potential energy. Then, the atom gets optically pumped into a potential well and the process starts over again. At this point, the analogy to the eponymous Greek myth, in which Sisyphus is punished by Hades, the ruler of the underworld, to carry a stone up the hill, just to see it roll down evoking the necessity to push it up again, becomes evident. Because of this analogy, cooling mechanisms which involve this scheme are called *Sisyphus cooling*. To understand this cooling technique, it will be qualitatively discussed in the low intensity regime with a red detuning and a transition $J \rightarrow J' = J + 1$. After the basic effect is explained blue detuned molasses, necessary to cool atoms on a $J \rightarrow J' = J$ transition, will be considered.

Low-Intensity Sisyphus Cooling

A lithium atom is considered to move slowly ($T \approx T_{\text{Doppler}}$) along the z-axis (quantization axis) in a standing wave, which is formed by two counter-propagating, orthogonally linearly

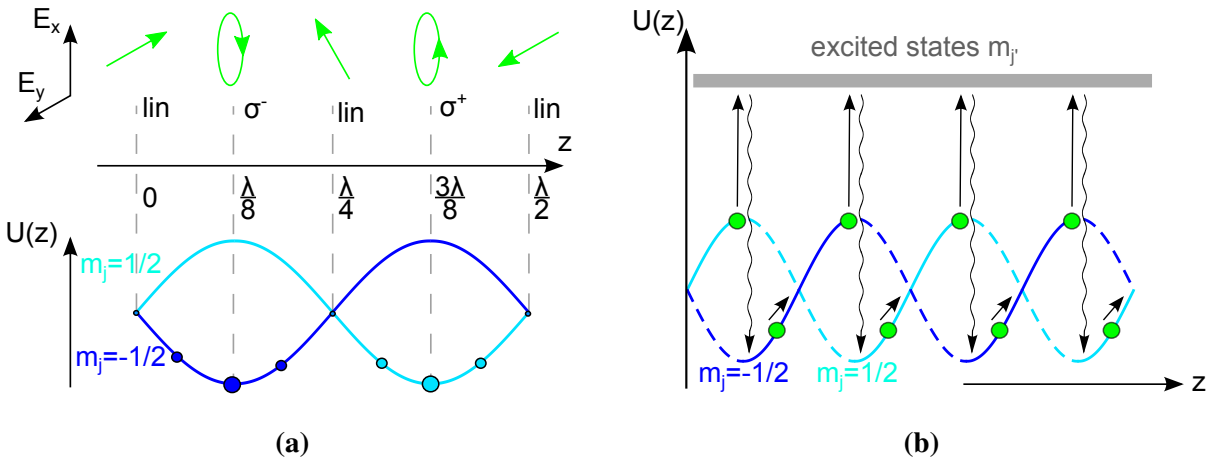

Figure 4.1. Low intensity Sisyphus cooling scheme. Panel (a) shows the polarization gradient of the electric fields E_x and E_y (top) and the resulting potential $U(z)$ seen by the atom (bottom) in dependence of the position z. The gray dashed lines indicate same points in position and polarization σ, lin. The filled circles of different sizes illustrate the steady state populations of the different sublevels $m_\mathrm{j} = 1/2$ and $m_\mathrm{j} = -1/2$. Panel (b) depicts the Sisyphus cooling process for an atom (green circles) moving along the z axis. The gray shaded area at the top illustrates the excited state manifold $m_\mathrm{j'}$.

polarized laser beams with electric field vectors described by

$$\mathbf{E}_1(z) = E_0 \frac{\hat{\mathbf{e}}_\mathrm{x} + \hat{\mathbf{e}}_\mathrm{y}}{\sqrt{2}} e^{ikz} \text{and} \tag{4.1}$$

$$\mathbf{E}_2(z) = E_0 \frac{\hat{\mathbf{e}}_\mathrm{x} - \hat{\mathbf{e}}_\mathrm{y}}{\sqrt{2}} e^{-ikz} \tag{4.2}$$

respectively. The laser beams are of low intensity $\Omega \ll \Gamma$ and are red detuned $\Delta < 0$. The summation of these two electric fields

$$\mathbf{E}(z) = E_0\sqrt{2}\left[\sin\left(kz + \frac{\pi}{4}\right)\left(\frac{\hat{\mathbf{e}}_\mathrm{x} + i\hat{\mathbf{e}}_\mathrm{y}}{\sqrt{2}}\right) + \cos\left(kz + \frac{\pi}{4}\right)\left(\frac{\hat{\mathbf{e}}_\mathrm{x} - i\hat{\mathbf{e}}_\mathrm{y}}{\sqrt{2}}\right)\right] \tag{4.3}$$

describes a superposition of a σ^+ and a σ^- standing wave with nodes of one standing wave coinciding with antinodes of the other one. Figure 4.1 (a) illustrates the spatially varying polarization, light shift and steady state population of the ground states $m_\mathrm{j} = \pm 1/2$ of a ^{6}Li atom at rest. At a position $z = n \times \lambda/4$, with $n \geq 0$ being an integer, the light has a linear polarization whereas at $z = m \times \lambda/8$, with $m > 0$ being an odd integer, the polarization is σ^- and σ^+, respectively. Due to the different polarizations, the light addresses different states with different transition rates dependent on the position of the atom. Thus the light shifts of the energy levels also vary in space.

To investigate the **Steady-State Population**, let us assume the atom to be at rest. If it is at a position $z = \lambda/8$ where the light has σ^- polarization, the transition strengths indicate that the light shift (negative, because $\Delta < 0$) is three times bigger for the $m_\mathrm{j} = -1/2$ than for the $m_\mathrm{j} = 1/2$ state. Due to the fact that only $\Delta m_\mathrm{j} = -1$ transitions can be addressed by this polarization, in steady-state all the atoms will populate the $m_\mathrm{j} = -1/2$ state. The exact opposite

happens at a position $z = 3\lambda/8$, where the light is σ^+ polarized. If, on the other hand, $z = \lambda/4$, the linear polarization of the light leads to an equal population of the two ground states.

The **Cooling Scheme** is illustrated in Figure 4.1 (b). An atom in the state $m_j = 1/2$ is considered to start at the position $z = 0$. It moves in the z-direction and climbs the potential hill while losing kinetic energy. As it reaches $z = \lambda/8$, it absorbs a σ^- polarized photon to go over to the excited state $m'_j = -1/2$. If it then decays into the $m_j = -1/2$ sub-level, it finds itself in a potential valley, where it climbs up the potential hill and again loses kinetic energy. As the atom reaches the position $z = 3\lambda/8$, the absorption of a σ^+ polarized photon leads to a transition to the $m'_j = 1/2$ excited state. The final spontaneous decay into the $m_j = 1/2$ ground state closes the cooling cycle. The atom undergoes many of these cycles, loses kinetic energy and therefore gets cooled.

It should be noted that the process, in which the atom absorbs a photon at a potential valley and ends at a potential hill after emitting, would lead to heating. Because of the selection rules these transitions are dipole-forbidden and therefore suppressed.

Blue-Detuned Sisyphus Cooling

Again, a lithium atom is considered to move slowly along the z-axis in a standing wave with a polarization gradient described as in equation (4.3). The difference to the above explained mechanism is that we consider a transition $F \rightarrow F' = F$. For the sake of simplicity, we will use the model with $F = 1/2$. The light shifts of the energy levels result in heating of the atomic cloud if the detuning of the laser beams is negative. The atom is rolling down more hills than climbing them. If the detuning is chosen to be positive $\Delta > 0$ this effect is reversed.

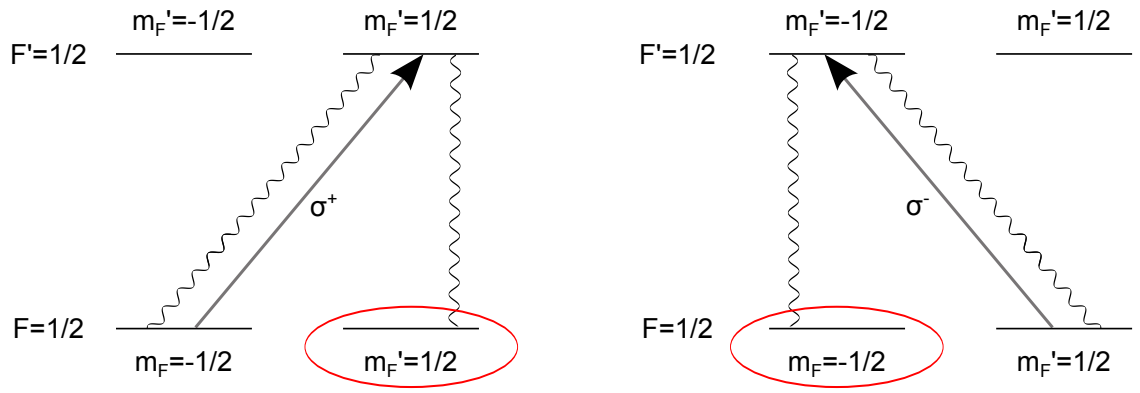

Figure 4.2. F=1/2 to F'=1/2 transition for different polarizations. Panels (a) and (b) illustrate the transitions between the ground state sublevels $m_F = 1/2, -1/2$ and the excited state sublevels $m'_F = 1/2, -1/2$. In panel (a)/(b) the standing wave has σ^+/σ^- polarization. The red ellipses mark states that are not coupled to the light. Wavy lines indicate the possibility for a spontaneous decay into either of the ground states.

The atoms are cooled due to the Sisyphus effect that arises in this blue detuned molasses for the transition $F \rightarrow F' = F$. For the fact that neighboring hyperfine levels would contribute

to heating effects if they are coupled to the light field, the laser beams have to be well detuned. In the case of 6-lithium, the excited state hyperfine splitting is on the order of $\Delta_{\text{HFS}} = 2\pi \times 26\,\text{MHz} \approx 4\,\Gamma$. The hyperfine states are resolved but they are close and therefore they can give rise to higher temperature. In recent experiments [11, 12] a detuning of a few times the linewidth $\Delta \approx 4 - 8\,\Gamma$ was chosen for blue Sisyphus cooling. To address the desired states properly, the intensity has to be increased.

Figure 4.2 illustrates the transition from $2^2S_{1/2}\ F = 1/2$ to $2^2P_{1/2}\ F' = 1/2$ in a lithium atom for two different polarizations of the light. In Figure 4.2 (a) (4.2 (b)) the light has σ^+ (σ^-) polarization. Atoms in the $m_{\text{F}} = 1/2$ ($m_{\text{F}} = -1/2$) ground state cannot absorb another photon because there exists no dipole-allowed transition. This state is not coupled to the light field anymore. For the fact that there exist uncoupled states, the scattering rate is reduced relative to the bright red-detuned molasses and the name "gray molasses" becomes evident.

An intuitive cooling limit for both the red and the blue detuned molasses is reached as the atom does not posses enough kinetic energy to climb the hill, and consequently, gets trapped in the optical potential wells. The height of these potential wells is dependent on the intensity of the laser, which cannot be decreased to an arbitrarily low value. However, if a photon is spontaneously emitted the atom gets a recoil

$$p_{\text{r}} = \hbar k, \tag{4.4}$$

which consequently limits the lowest achievable temperature [29]. The lowest achievable temperature by Sisyphus cooling can be approximated to be within a few recoil temperatures

$$T_{\text{r}} = \frac{(\hbar k)^2}{2Mk_B}. \tag{4.5}$$

Typically one can reach $5 - 30 \times\ T_{\text{r}}$ [30, 31]. The recoil temperature of ^{6}Li is $T_r = 3.5\,\mu$K.

The effect of different laser light polarizations on the Sisyphus cooling scheme goes beyond the scope of this thesis and shall not be discussed here. Predictions for a cooling limit, the effect of different polarizations and calculations of the Sisyphus effect can be found in [32–35].

4.2 Sub-Recoil Cooling

To cool atoms below the recoil temperature, it is necessary to prevent the atoms with momentum $p < p_{\text{r}}$ from absorbing another photon that could increase their momentum. This can be achieved by using so-called *dark states*. If an atom occupies a dark state, it becomes transparent for the laser light and does not undergo absorption and emission processes anymore.

The sub-recoil cooling method presented in this thesis is called *velocity-selective coherent population trapping* (VSCPT). As the name suggests, atoms in a certain velocity class - i.e. velocities of $[v - \delta v, v + \delta v]$ - get trapped in a dark state. Figure 4.3 illustrates a configuration of ^{6}Li where such a dark state can occur. In this three-level system two transitions are dipole allowed - $|1\rangle$ to $|3\rangle$, $|2\rangle$ to $|3\rangle$ - and the third $|1\rangle$ to $|2\rangle$ is dipole forbidden. A bi-chromatic laser field, with Rabi-frequencies Ω_1 and Ω_2, couples each of the ^{6}Li hyperfine ground states $2^2S_{1/2}$ $F = 1/2$ ($|1\rangle$) and $F = 3/2$ ($|2\rangle$) separately to the excited hyperfine state $2^2P_{3/2}\ F = 3/2$ ($|3\rangle$). If the relative detuning of the two laser beams, $\Delta = \Delta_1 - \Delta_2$, matches the energy splitting of

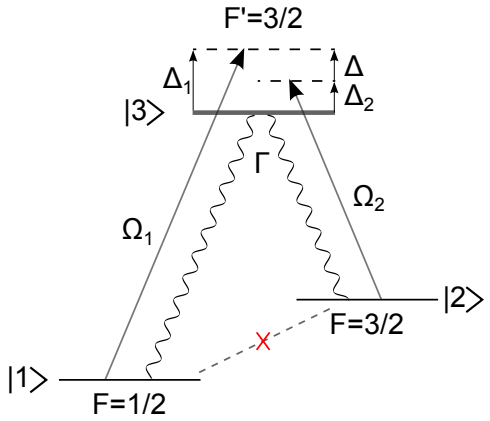

Figure 4.3. Lambda System in ^{6}Li. The two ground states are $F = 1/2$ ($|1\rangle$), and $F' = 3/2$ ($|2\rangle$) are coupled to the excited state $F = 3/2$ ($|3\rangle$) by two lasers with Rabi frequencies Ω_1 and Ω_2. The decay rate of the excited state is Γ. Δ is the relative detuning between the two laser beams with individual detunings Δ_1 ans Δ_2.

the hyperfine ground states

$$E_2 - E_1 = \hbar\omega_1 - \hbar\omega_2, \tag{4.6}$$

the so-called *Raman condition* is fulfilled. One photon (e.g. $\hbar\omega_1$) is absorbed and the emission of another photon (e.g. $\hbar\omega_2$) is stimulated. The atom goes from one ground state to the other ground state [36]. A detailed calculation of the excited state population and the coherence by the use of optical-Bloch equations can be found in [37].

To explain the processes that lead to a cooling effect, we use the dressed-atom approach. As in the Sisyphus scheme, it is assumed that the light beams build up an optical molasses of two counterpropagating beams along all three dimensions. The three eigenstates of the coupled system are superpositions of the bare atomic eigenstates. As the Raman condition is fulfilled, one of these states Ψ_D has no excited state contribution

$$|\Psi\rangle_\mathrm{D} = c_1 |1\rangle + c_2 |2\rangle = \frac{\Omega_2 |1\rangle - \Omega_1 |2\rangle}{\sqrt{\Omega_1^2 + \Omega_2^2}}. \tag{4.7}$$

Because this eigenstate is in a coherent superposition of two ground states, it can neither emit nor absorb a photon and is therefore a dark state.

If an atom moves with a velocity v it experiences a Doppler shift. In the rest frame of the atom, the frequency of the light is shifted and thus the Raman condition is no longer fulfilled. The atoms have to undergo absorption and emission processes to change their velocity. This can be achieved by e.g. Sisyphus cooling. Eventually they reach $v = 0$ m/s where they accumulate in the dark state.

It can be assumed that if the two lasers are applied long enough at a relative detuning $\Delta = 0$, all the atoms will be stored in the dark state and a temperature of $T = 0$ seems to be reachable. Though, certainly there are limitations to this dark-state trapping: First, every interaction of the atom with its surrounding can change the atom's momentum to a non-zero value and it will couple to the light field again. Second, if the two lasers are not coherent the lifetime of the dark

state is going down. To understand the second argument we have a closer look at the probability amplitude (PA) to have an absorption from $|1\rangle$ ($|2\rangle$) to $|3\rangle$. This amplitude equals the product of the PA of the atom to be in the ground state c_1 (c_2) and the PA to have an absorption out of this state, which is proportional to Ω_1 (Ω_2). For a dark state to occur, the PA to have an absorption from any ground state to $|3\rangle$ must vanish

$$\Omega_1 c_1 + \Omega_2 c_2 = 0. \tag{4.8}$$

This requirement is indeed fulfilled in equation (4.7). A dark state can be interpreted as a destructive interference of these amplitudes. For non-coherent laser beams the time evolution would no longer fulfill this requirement [36].

As a dark state, where atoms with low momentum accumulate, is involved in this cooling technique, the photon scattering rate is reduced in comparison to a red detuned bright molasses. Therefore the cooling scheme using blue detuned molasses and a dark state are also called "gray molasses".

4.3 Conditions for Sub-Doppler Cooling of Fermionic Lithium

Due to the fact that every atomic species has its unique energy-level structure, different cooling methods can be applied for different atoms. The level structure of ^{6}Li is shown in Figure 4.4. The linewidth $\Gamma_{D2} = 2\pi \times 5.87\,\text{MHz}$ [38] of the D2 transition to $2^2P_{3/2}$ is greater than the excited state's hyperfine splitting. This means that the hyperfine structure is not resolved and the hyperfine states can not be addressed individually.

In the FeLiKx-experiment at the University of Innsbruck, we achieve temperatures of $T \approx 230\ \mu K$ in the MOT that uses light on the D2 transition. This value is in fact already close to the Doppler temperature $T_\text{D} \approx 140\,\mu K$. To further lower the temperature of the atoms, a sub-Doppler cooling technique is needed. The unresolved hyperfine structure of the D2 transition would result in heating because the specific excited states cannot be addressed. Therefore the D1-transition, depicted in Figure 4.4, is considered.

In contrast, other alkali atoms such as Na or Cs do have a resolved hyperfine splitting at the D2-transition. Therefore, at sufficient low intensities of the optical molasses, sub-Doppler temperatures can be reached without any additional setup because Sisyphus cooling can arise there. In 1988 a group led by Bill Phillips[4] published a paper with following abstract:

> We have measured the temperature of a gas of sodium atoms released from "optical molasses" to be as low as $43\pm20\,\mu$K. Surprisingly, this strongly violates the generally accepted theory of Doppler cooling which predicts a limit of $240\,\mu$K. To determine the temperature we used several complementary measurements of the ballistic motion of atoms released from the molasses [39].

At that time the Doppler limit was thought to be the lowest by laser cooling achievable temperature of an atomic cloud. Due to the experimental work of the group around Steven Chu and the following theoretical description by a group led by Claude Cohen-Tannoudji, several different

[4] In 1997 William D. Phillips, Steven Chu, and Claude-Cohen Tannoudji were awarded the Nobel Prize "for development of methods to cool and trap atoms with laser light".

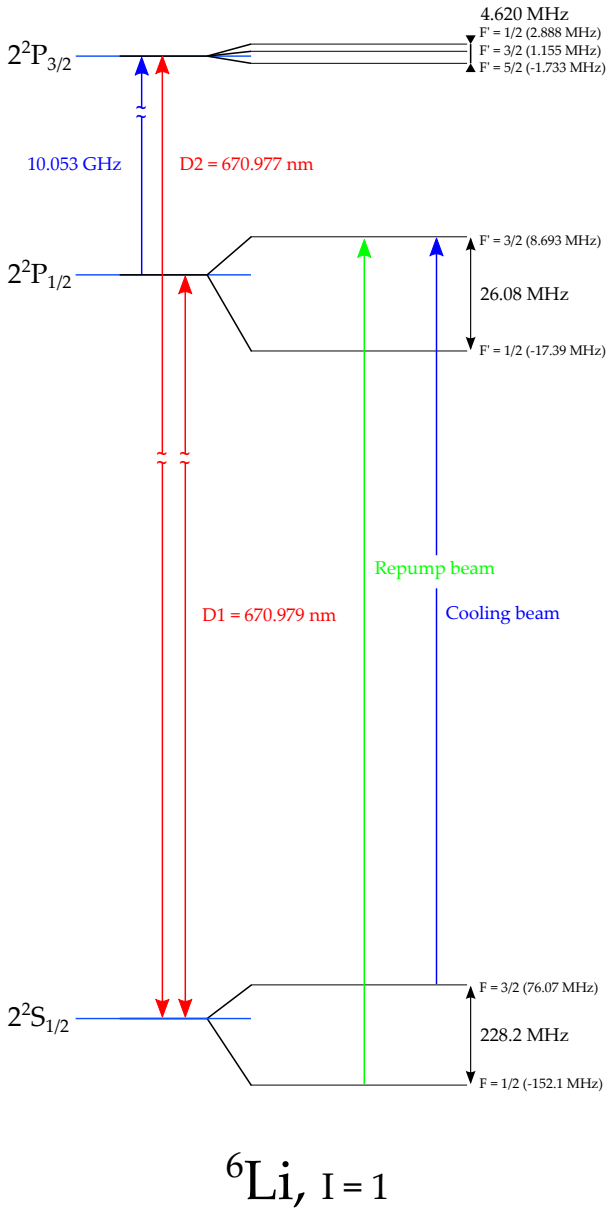

Figure 4.4. Hyperfine energy levels of 6-lithium. The D1 transition from $2^2S_{1/2}$ to $2^2P_{1/2}$ and the D2-transition from $2^2S_{1/2}$ to $2^2P_{3/2}$ are marked red. The nuclear spin is $I = 1$. The two different laser frequencies used in the gray molasses scheme are depicted as the cooling (blue) and repump (green) beam. Figure based on [8].

laser cooling techniques have been developed. Among others, the gray-molasses scheme used in this thesis.

The cooling scheme starts after a MOT. A three dimensional bichromatic optical molasses blue detuned from the D1-transition of ^{6}Li is then applied. The cooling effects can be interpreted as a Sisyphus effect and a dark state arising as the Raman condition is fulfilled.

Chapter 5

Laser Stabilization and Experimental Setup

In the experiment presented in this thesis, a $\lambda = 671\,\text{nm}$ diode laser system from Toptica (TA pro) is used. All frequencies are derived from this master laser by acousto-optical frequency shifting techniques. The master laser is locked to the Li D1 transition by modulation transfer spectroscopy (MTS) in a heated Li cell. The master oscillator light is then shifted and amplified to the frequencies necessary for the gray molasses cooling scheme. After this, the light is sent through an optical fiber to the experimental table, where the atoms are trapped.

This section describes the principle and the experimental setup of modulation transfer spectroscopy. After this, the setup for the sub-Doppler cooling stage is explained. The imaging procedure is described in the last section.

5.1 Modulation Transfer Spectroscopy

Modulation transfer spectroscopy [40] is a Doppler-free spectroscopic method, which can be applied to stabilize a laser at a desired frequency, in this case the D1 transition of ^{6}Li (illustrated in Figure 4.4). The theoretical model for this spectroscopy will be explained before the optical setup is shown.

Principle of MTS

A spectroscopy cell is heated to the temperature at which the atoms have a vapor pressure where the absorption signal is about $10\,\%$ of the transmitted signal (here $\sim 300\,^\circ$C). A laser beam is divided into a strong pump and a weak probe beam. Both beams are sent to the spectroscopy cell, from opposite directions, so that they overlap. By applying a triangular voltage signal to the piezo element of the Toptica laser, its frequency is tuned. Due to the Doppler effect, atoms with different velocities will be resonant to each of the laser beams for different frequencies. If the laser frequency approaches a value that coincides with an atomic transition frequency, the strong pump laser will be absorbed by atoms whose velocity component along the beam is zero. After this, the atoms will be saturated. Since the frequency of the probe beam is equal to that of the pump beam, the probe beam will then also strongly interact with the atoms in the same velocity class.

The interaction of the two beams with the same atoms leads to nonlinear effects. Modulation-transfer spectroscopy makes use of this non-linearity to produce a spectroscopy signal. With the aid of an EOM, sidebands at a frequency of $\nu_\text{s} = 18.5\,\text{MHz}$ are modulated onto the pump laser. As this modulation frequency is bigger than the natural linewith of the D1 transition of

6-lithium, we observe a broad error signal with a wide lock-in range. If the interaction between the atoms and the two laser beams is sufficiently non-linear, the modulation is transferred from the pump to the probe beam. This process is explained via four-wave mixing [41]. Two frequency components of the pump laser - one sideband ν_s and the carrier ν_c - are combined with the frequency of the probe beam via the non-linearity of the atoms. A fourth wave is then produced in the probe beam path, with an offset from the original probe beam by the pump modulation frequency.

After the spectroscopy cell, the probe beam is sent to a fast photodiode that detects the resulting amplitude modulation of the probe beam. This signal is then electronically converted to an error signal (see Figure 5.2), which is sent to a PID controller to stabilize the laser frequency.

It should be noted that there is a situation where atoms with a certain nonzero velocity interact with both beams. If we consider the hyperfine structure at the D1 transition (see Figure 4.4) of a 6-lithium atom, there exists a velocity for the atom where the pump is resonant to the $F = 3/2$ to $F' = 3/2$ transition and the probe is resonant to the $F = 1/2$ to $F' = 3/2$ transition. This happens if the master-laser output is at a frequency that matches the difference of the hyperfine splitting $\hbar\omega = E_3 - (E_2 - E_1)/2$. The modulation-transfer spectroscopy signal produced at this frequency is called a *crossover resonance*. It should be noted that there is a second crossover resonance at the D1 transition, namely for laser light resonant to the $F = 3/2$ to $F' = 1/2$ and the other to the $F = 1/2$ to $F' = 1/2$ transitions.

Experimental Setup of MTS

As a light source, the TA pro laser from Toptica, operated at $671\,\text{nm}$, is used. It consists of a laser diode and a tapered amplifier (TA). Each of these devices is followed by an optical isolator to prevent it from being affected by back reflections. The 20 mW seeding light of the TA is amplified to ~ 500 mW. The output power of the TA pro - after the optical isolator - is $\sim 400\,\text{mW}$. It is sent through a $\lambda/2$ waveplate followed by a polarizing beam splitter, which results in the two paths as illustrated in Figure 5.1. About 390 mW, are sent to a fiber that transports the light to the SDC setup. The remaining 10 mW are used for the MTS.

The spectroscopy beam is split into a strong pump and a weak probe beam by a polarizing beam splitter. The relative strength of these two beams can be adjusted with a $\lambda/2$ plate. The pump beam then passes through an electro-optical modulator (EOM) which is driven by the amplified signal from a voltage controlled oscillator (VCO) at $18.5\,\text{MHz}$. By passing through the EOM, the pump beam acquires two sidebands $\pm 18.5\,\text{MHz}$ away from the carrier frequency of the original laser beam. Once the pump beam passes through the next PBS, it enters the spectroscopy cell.

The lithium spectroscopy cell is wrapped with heating wires to get the desired temperature of $\sim 300\,^\circ\text{C}$. The cell is water cooled to prevent the surrounding optics from drifting due to heating. After the pump beam passes the cell, it is led to a beam dump.

The probe beam, which has $1/10$ of the power of the pump beam, enters the spectroscopy cell, as illustrated in Figure 5.1. If (and only if) the hyperfine-condition is fulfilled and the two beams are overlapped, the modulation of the pump is transferred to the probe beam via a four-wave mixing process. The modulation of the probe beam is detected by a photodiode (PD) where the Doppler-free absorption signal is observed. With an electronic circuit, the error signal can then be produced. In this thesis, a home built "phase detector", which consists of a

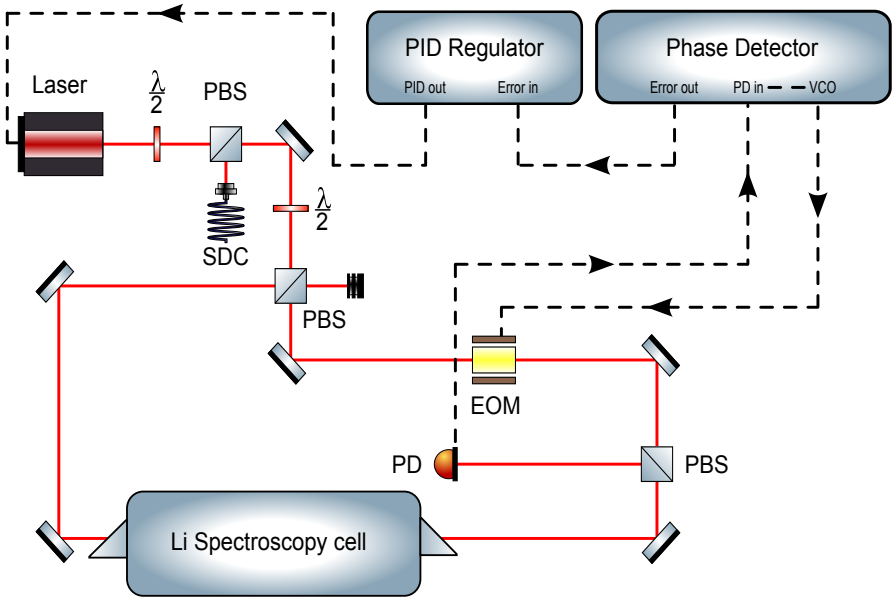

Figure 5.1. Modulation-transfer spectroscopy setup. The red lines correspond to the laser path and the black dashed lines show the electrical connections.

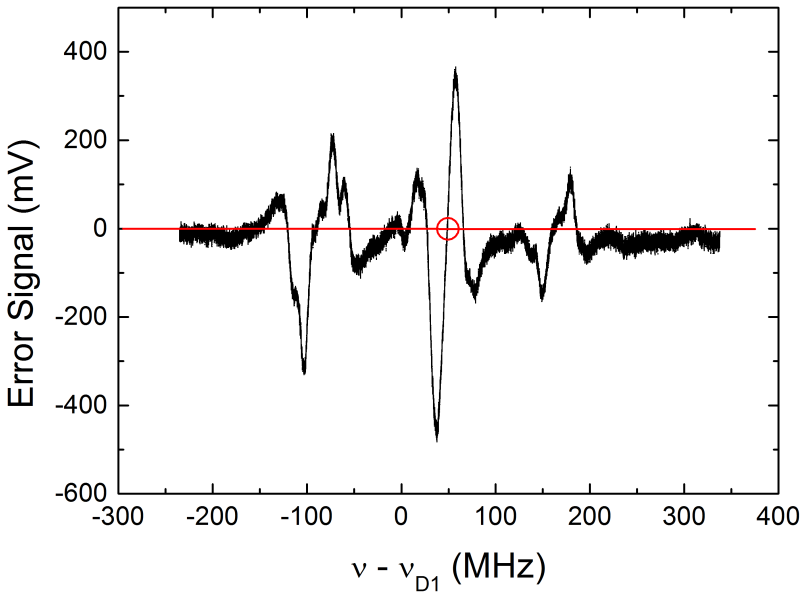

Figure 5.2. Error signal as a function of the laser frequency ν relative to the D1 transition frequency ν_{D1}. The intersection of the red line at 0 V and the error signal, marked by a red circle, indicates the lock point.

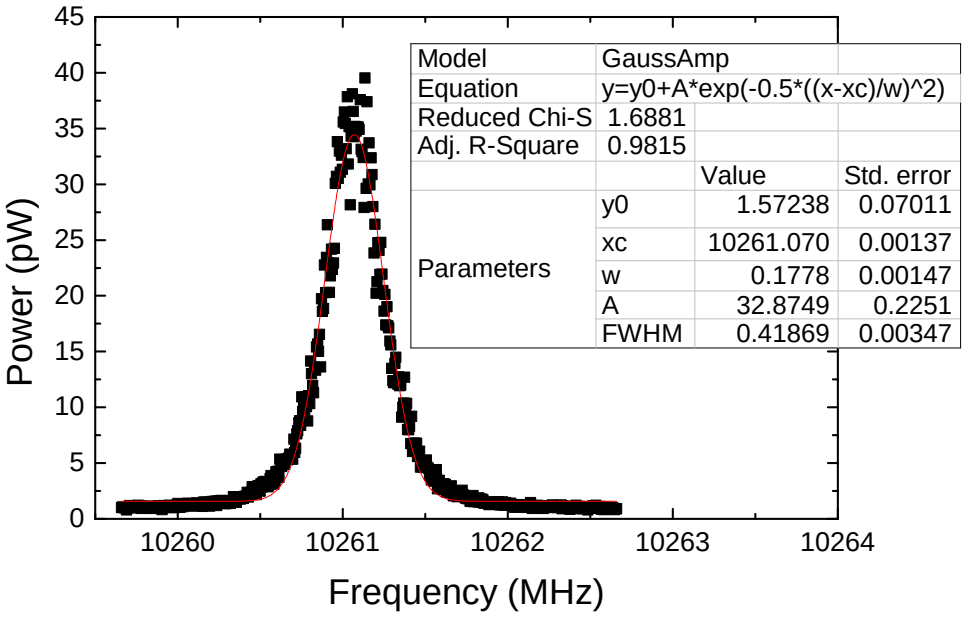

Figure 5.3. Beat signal between lasers locked to the D1 and D2 transition. The red fitting curve follows a Gaussian distribution.

VCO and an electronic mixer with adjustable phase, and a a PID controller from Toptica (PID 110) are used. The signal from the PD is electronically multiplied with the output of the VCO that also feeds the EOM, by the electronic mixer. With this, the error signal is produced.

Figure 5.2 depicts the error signal, which is sent to the PID module. The zero point of the horizontal axis corresponds to the frequency ν_{D1} of the D1 transition $2^2S_{1/2}$ to $2^2P_{1/2}$. The frequency scale is determined by a beat measurement, which is explained in the next paragraph. One can see, that there are three frequencies at which the laser seems to be on resonance with a transition of the D1 spectrum of lithium. The two outer resonance peaks are separated by approximately 230 MHz, which corresponds to the hyperfine splitting of the ground state of ^{6}Li (see Figure 4.4). The middle resonance peak consists of the two crossover resonances appearing as a result of the four energy levels present at the D1 transition of 6-lithium. One could think that the error signal should consist of six contributions, namely the four resonant transitions and the two crossover resonances. For the reason that the excited state hyperfine structure is not resolved, there appear only three signals. The controller stabilizes the laser to a frequency that corresponds to the mean value of this two crossover resonances. The horizontal position of the locking point in Figure 5.2 - indicated by the red solid line - is determined by subtracting the background from the PID output signal.

After this procedure the laser is stabilized to the frequency of the D1-transition of ^{6}Li. The upper bound of the linewidth of the laser can be determined using a beat measurement. For this purpose, the D1-stabilized laser beam is overlapped with a reference laser beam and observed on a photodiode. At the FeLiKx experiment there exists a laser system stabilized to the D2 transition of ^{6}Li. A part of this laser beam, which is used for imaging the atoms, is taken as the reference signal. The frequency difference between the D1- and the D2-transition is larger

than 10 GHz and therefore a photodiode with a bandwidth of 12 GHz is used to record the beat signal.

Figure 5.3 shows the power spectrum of the signal from the photodiode detecting the beat between the D1 cooling master laser and the imaging light extracted from the D2 master laser of the FeLiKx setup. The calculated frequency difference between these two lasers is $\sim 10262 \pm 1$ MHz. We fit the obtained spectrum to a Gaussian model and obtain the center frequency $\nu_{\text{beat}} = 10261$ MHz, which matches the calculation. The width of the Gaussian fit is $2w = 356$ kHz. The squared width of the obtained beat signal consists of the sum of the squared single linewidths. If we assume that both lasers fluctuate in the same way, we can estimate the linewidth to $\delta\nu \approx 250$ kHz.

5.2 Sub-Doppler Cooling

The optical setup for lithium of the FeLiKx experiment is separated on two different optical tables. The first one is the optical table where the laser stabilization takes place and the desired laser frequencies are prepared. The second one is the main table where the ^{6}Li atoms are first captured in a magneto-optical trap, then their ρ_{psd} is increased by the gray molasses, and then they are cooled to temperatures in the nK regime, by forced evaporation. Therefore, this section will be split into two parts, namely the laser setup and the integration of the additional laser beams into the trap setup.

Laser and Frequency Control Setup

Two laser beams with different frequencies are required for the gray molasses scheme used in this thesis: the repump beam and the cooling beam (as depicted in Figure 4.4). The setup is built in a manner that a wide parameter range can be accessed. Following requirements have to be fullfiled:

- The frequencies of both beams must be jointly adjustable in a range of a few times the linewidth Γ.
- The frequency of the repump beam must be separately adjustable in a range of a few Γ.
- A frequency separation, of the two laser beams, that matches the ground state hyperfine splitting must be achievable.
- Both beams should be blue detuned with respect to their resonance frequency by a few Γ.
- The intensity of the cooling beam at the position of the atoms has to exceed the saturation intensity I_{SAT}, while the intensity of the repump beam can be a few percent of the cooling beam.
- The intensity ratio between the two beams should be adjustable.
- It must be possible to switch on/off both laser beams fast $t < 10\,\mu$s and independently.

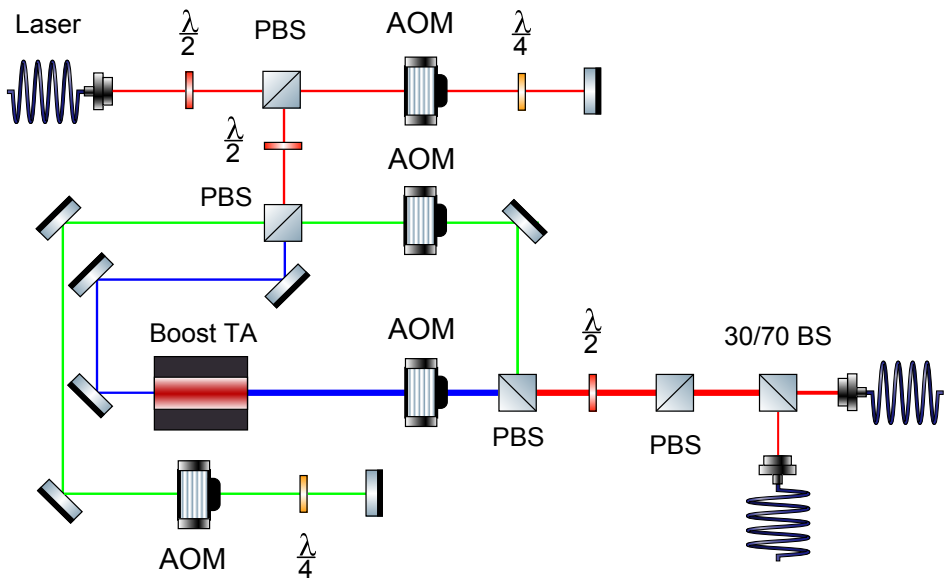

Figure 5.4. Setup for sub-Doppler cooling beams. The blue (green) lines describe the optical path of the cooling (repump) beam whereas the red lines correspond to the combined beam.

The optical setup used to produce the two beams, according to these requirements, is illustrated in Figure 5.4.

The frequency-stabilized laser beam enters the setup through an optical fiber. This fiber has two purposes. First, the non-Gaussian intensity profile at the output of the TA gets "cleaned" by propagating through the fiber, which is necessary to operate the following optical elements in a power efficient manner. Second, if the Master laser needs to be maintained and the output slightly changes its propagation direction, the only thing that needs to be realigned is the coupling into the optical fiber. The rest of the optical setup does not have to be realigned.

With the aid of a $\lambda/2$ plate, the whole beam is sent through the first PBS and is frequency shifted by an $80\,\mathrm{MHz}$ acousto-optic modulator (AOM). The first order of refraction of this AOM is sent back, building a double pass configuration with a total frequency shift of $160\,\mathrm{MHz}$. The beam passes the $\lambda/4$ plate two times and will therefore be reflected by the PBS to move downwards, as shown in Figure 5.4. At the second PBS the beam is split into a cooling (blue) and a repump (green) beam. The former is adjusted via the $\lambda/2$ plate to have a light power of $\sim 20\,\mathrm{mW}$ to seed the tapered amplifier (Boost-TA from Toptica). About $400\,\mathrm{mW}$ of optical power are then sent to an AOM in a single pass configuration. The resulting -1 diffracted order is shifted in frequency by $-230\,\mathrm{MHz}$ relative to the input beam. The repump beam, on the other hand, is sent to a $110\,\mathrm{MHz}$ AOM in a double-pass configuration, to shift its frequency by $220\,\mathrm{MHz}$. Due to the $\lambda/4$ plate following this AOM, which is passed two times by the laser beam, it will pass the second PBS to reach the last AOM in a single-pass configuration and to be shifted by $220\,\mathrm{MHz}$.

After all the AOMs are passed, the two beams get overlapped on a PBS. A subsequent $\lambda/2$ plate regulates the ratio between the two beams which will then pass the last PBS with same polarization. The $30/70$ beam splitter ensures that $30\,\%$ of the beam go into one fiber and $70\,\%$

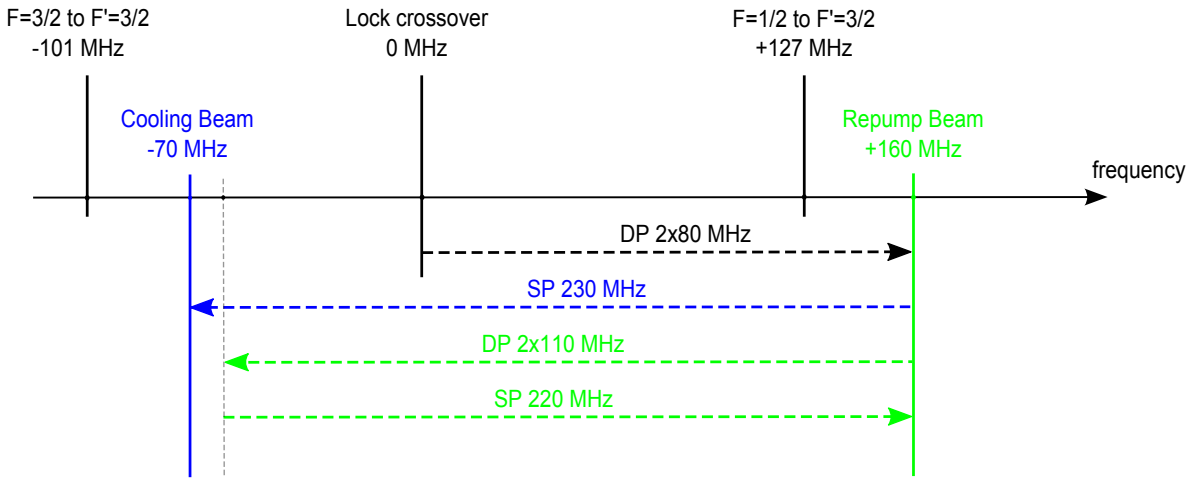

Figure 5.5. Illustration of the frequency shifts. The lock point corresponds to the mean frequency of the crossover resonances. The blue (green) line marks the cooling (repump) beam. All frequencies are either shifted by an AOM in a double pass (DP) or in a single pass (SP) configuration.

into the other. The two different fibers are chosen to cover the two horizontal directions with one and the vertical with the other one, as explained in section 5.2.

With this setup all the requirements are fulfilled. Figure 5.5 illustrates the frequency shifts of the repumper and the cooler. The solid lines depict the two atomic transitions (black), the mean of both crossover resonances (black), the cooling beam (blue), and the repump beam (green). Dashed horizontal lines show the frequency shifts. The black DP is used two shift both beams jointly. At this point the cooling beam is shifted to its final frequency with the blue SP AOM, which is also used to switched off the beam. It is shifted from the cooling transition (F=3/2 $\rightarrow$ F'=3/2) by about $31\,\mathrm{MHz}$, which corresponds to a blue detuning of $5.3\,\Gamma$. To make sure that the repumper is tunable another DP is needed (green). Finally the right frequency of this beam is achieved by the last SP (green). The second use of this SP is to switch off the repumper. The two beams are separated by $230\,\mathrm{MHz}$, which approximately corresponds to the hyperfine splitting of the ground state of ^{6}Li.

Every AOM in this setup is fed by a different direct digital synthesizer (DDS) with its desired frequency. The control system is based on a parallel bus system in which a National Instruments NI6533 digital output card connects the computer with the bus system. A detailed explanation of the electronic setup to control different cycles in the experiment can be read in [8]. With this it is possible to drive the AOMs independently and therefore to shift the frequency of the repumper and of the cooler independently.

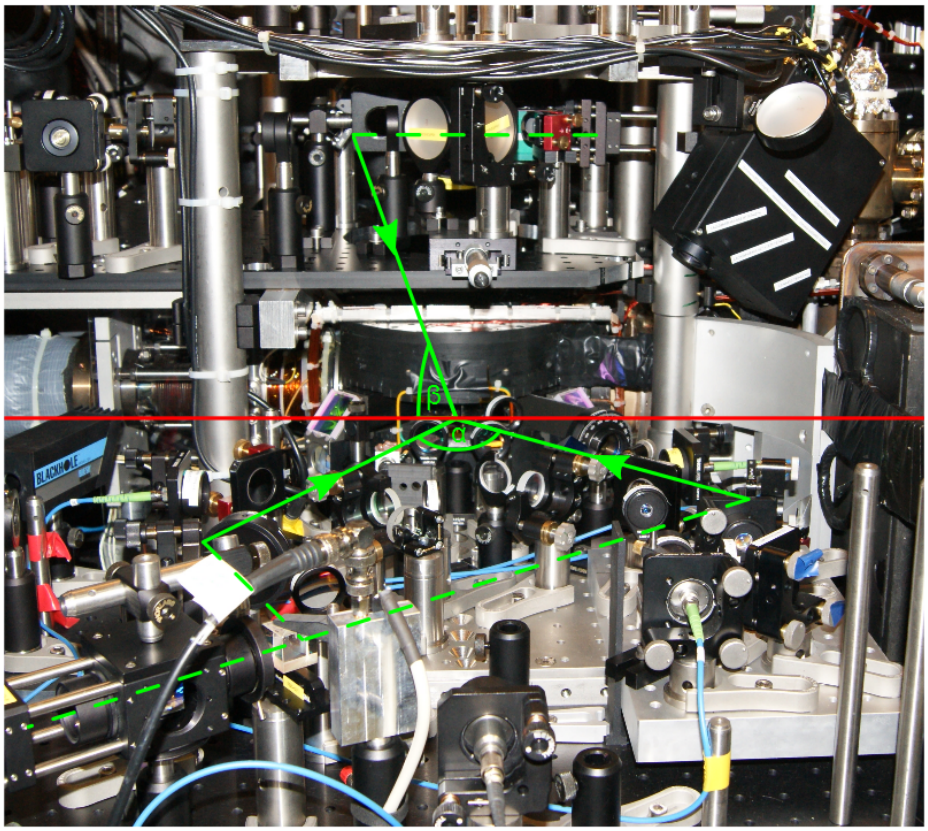

Figure 5.6. D1 beams at main table. The direction of the D1 beams at the main table is shown by the green lines. The angle between the two beams in the horizontal plane is $\alpha = 42°$. The angle of the vertical laser beam with respect to the horizontal plane (red solid line) is $\beta = 71°$.

Integration into the Trap Setup

As mentioned before, the two independently tunable laser beams are overlapped and transported to the main table in two optical fibers. One of them carries $70\,\%$ of the whole power, while the rest is sent through the other. The former covers the two dimensions of the horizontal plane while the latter provides light for the vertical direction, as illustrated in Figure 5.6. To obtain the desired beam properties, a Thorlabs "cage system" is used. This cage system eases alignment while providing easy access for changes in beam size and collimation. In this experiment, the beams for D1 cooling have independent optical access to the atoms, allowing flexibility in beam size, polarization and collimation. Due to the limited optical access at the main table, the cooling and repump beams are not perpendicular to each other, as can be seen in Figure 5.6.

After exiting the fiber, the horizontal beam is split by a PBS. After this, there is space for an optional $\lambda/4$ plate to change the polarization from linear to circular. The beams are retro-reflected after passing the glass chamber. A $\lambda/4$ plate is inserted right in front of the retro-reflecting mirror to change the polarization of the backwards traveling beam. With this setup we have the freedom to choose the polarization and study its influence on the cooling mechanism. The vertical beam passes similar optics. After aligning the beams to hit the atoms, the beam diameter is fixed. The beam waists for the horizontal and vertical laser beams are

$\sigma_{\text{hor}} = 4.2\,\text{mm}$ and $\sigma_{\text{ver}} = 3.9\,\text{mm}$, respectively. They are measured by the Thorlabs Camera Beam Profiler BC106-VIS.

5.3 Imaging

The imaging system used to determine temperature and atom number of the laser cooled cloud has been already an integrated part of the FeLiKx experiment since the construction of the machine [8]. Therefore the consideration here is restricted to the calibration and determination of the interesting values and its errors, namely the temperature and the atom number.

Absorption Imaging

The absorption imaging of atoms in this thesis is performed using an ANDOR Luca R DL 604M - OEM camera. A bichromatic laser beam resonant two the D2 transition of ^{6}Li (F=3/2 $\rightarrow$ F'=1/2 and F=1/2 $\rightarrow$ F'=3/2) is shone onto a CCD chip. The CCD chip is $1004\,\text{px}$ high and has an active area with a width of $1002\,\text{px}$. We installed a razorblade in front of the chip to cover $716\,\text{px}$ of the active area. To calculate the optical density of the atoms, which is needed to determine the atom number and the temperature, four shots are taken.

- The atoms are trapped, the imaging light has passed the atoms, and is detected on the CCD camera (I_1).
- The camera shifts the image by $286\,\text{px}$ to the area which is covered by the razorblade.
- The imaging light is directed on the CCD camera without any trapped atoms (I_3).
- The camera reads out the two images.
- After a waiting time of about $1\,\text{s}$ and no imaging light is applied, the camera again shifts the image to the area which is covered by the razorblades. Then The imaging light is applied. After that, the camera reads out the two images. With this measurement, the background of the first image (with atoms) is determined (I_2).
- To get the background I_4 of the second image (without atoms) the same procedure is carried out but the imaging light is applied before the shift.

It should be noted that there is no readout between the two images I_1 and I_3 are taken. Therefore they have a different background. This is taken into account by I_2 and I_4.

According to Beer's law, the intensity I of a laser beam after passing an absorbing medium (atoms) is proportional to the intensity of the original beam I_0

$$I = I_0 e^{-\tau}, \tag{5.1}$$

with a proportionality factor that is given by the optical depth τ of the atoms. To measure the optical depth in an experiment,

$$\tau = -\ln\left(\frac{I}{I_0}\right) = -\ln\left(\frac{I_1 - I_2}{I_3 - I_4}\right) \tag{5.2}$$

the background light is taken into account. Figure 5.7 shows an image taken by the ANDOR camera, where the atoms had time to expand for $4\,\text{ms}$.

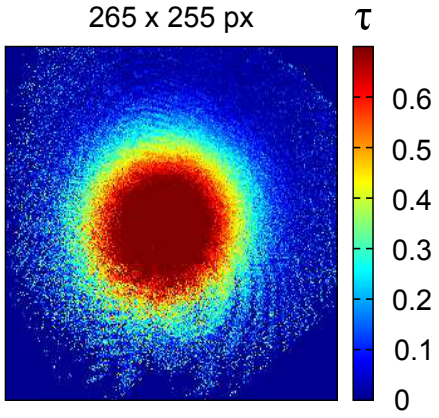

Figure 5.7. Image of an atomic cloud. The colors indicate the magnitude of the optical depth of the cloud. The size of the image is 265×255 px. The size of one pixel is $30.5 \times 30.5\,\mu\text{m}^2$.

Chapter 6

Characterization of the Sub-Doppler Cooling Technique

The goal of the sub-Doppler cooling stage in the FeLiKx experiment is to improve the phase-space density, and thus to provide better starting conditions for subsequent evaporative cooling in an optical dipole trap. To achieve this, we must lower the temperature without expansion of the atom cloud. Moreover, we have to achieve that no atoms are lost from the cooling process. To characterize the gray-molasses cooling technique introduced in this thesis, many parameters can be varied. In this chapter there will be a discussion about these parameters and how they are adjusted to find optimized settings for the purpose of this experiment.

First the extraction of temperature and atom number from images is discussed and the variable parameters will be introduced. After that, the parameters will be varied to characterize the cooling system.

6.1 Data Fitting and Errors

The Li atoms are detected by absorption imaging, as was described in chapter 5. Absorption imaging provides information about the optical depth, which is proportional to the column density of the atomic cloud. The obtained images are analyzed by a MATLAB program, which has been implemented as a standard routine in our data analyzing software. For each pixel, the optical depth is calculated from images such as the one depicted in Figure 5.7. Figure 6.1 (a)illustrates an image taken after $t_{\text{tof}} = 4\,\text{ms}$ and plotted in MATLAB, in which one row of pixels is marked by a white dashed line. The sum of the optical depths of the pixels in each row, τ_{hor}, is shown as a function of the column index in Figure 6.1 (b). The data is then fitted by a Gaussian distribution. The width of this distribution corresponds to the width of the atomic cloud σ_{c} and is used to determine the temperature.

One pixel of the camera corresponds - according to the datasheet - to $8 \times 8\,\mu$m. The imaging light gets magnified on its way to the camera and therefore we need to measure the magnification factor to get the real size of the cloud. We image the cloud at different times of flight and plot the position of the cloud in dependence of the time of flight. For the fact that the atoms are accelerated by the Earth's gravitation, their vertical center of mass position in time is described by $x(t) = x_0 + vt + t^2 g/2$, in which x_0 is the initial cloud position. From fitting a parabola $x_{\text{fit}}(t) = a + bt + t^2 c/2$ we can extract the constant c and compare it to the gravity acceleration g. The deviation between these two values results in the magnified pixel size $u = 30.5 \pm 1\,\mu$m. The uncertainty of the magnified pixel size gives a systematic error in temperature of

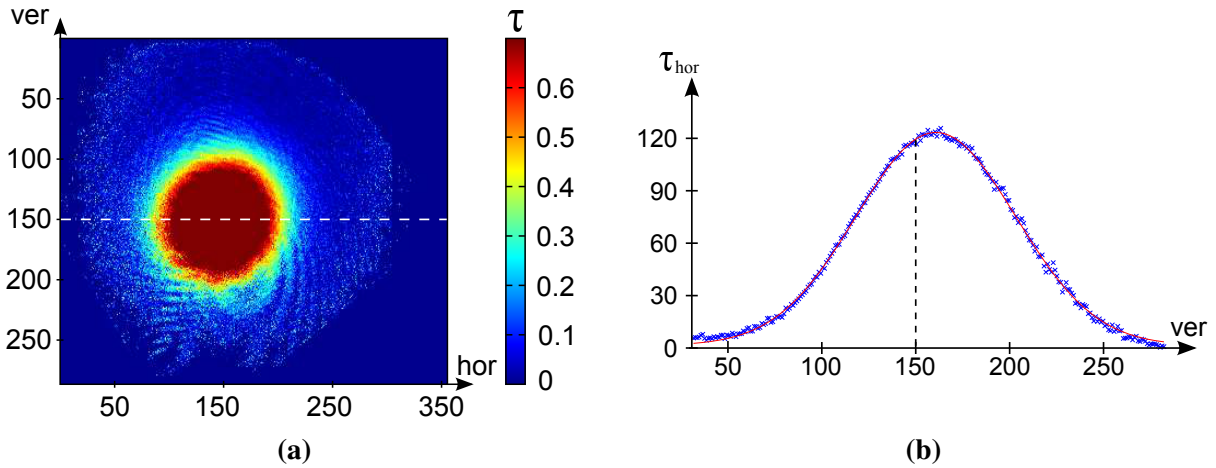

Figure 6.1. Analysis of imaging data. Panel (a) shows the image of an atom cloud extracted from the MATLAB program. The color of every pixel states the optical depth τ. The white dashed line marks one of the vertical (ver) rows of pixels. The sum of these pixels corresponds to the point in panel (b) that is marked by the black dashed line. The summation of all rows in (a) corresponds to the blue crosses in (b). The vertical axis in (b) states the sum of the optical depths τ_{hor} of every pixel in horizontal (hor) direction. A Gaussian distribution (red solid line) is fitted to the data.

$\Delta T/T = \pm 6.5\,\%$. It should be noted that this error influences all values in the same way. It has no contribution to the statistical error bars presented in this thesis.

The temperature of the atom cloud is determined by a time of flight (TOF) method. After all the cooling steps are done, the D1 laser light is switched off, and the atoms are allowed to expand. With the assumption of a Gaussian-shaped cloud, the measured cloud size is

$$\sigma_{\text{c}}^2 = \sigma_0^2 + \sigma_{\text{v}}^2 t_{\text{TOF}}^2, \tag{6.1}$$

where σ_0 corresponds to the cloud size at time $t_{\text{TOF}} = 0\,\text{ms}$, and $\sigma_{\text{v}} t_{\text{TOF}} = \sqrt{k_{\text{B}} T/m}\; t_{\text{TOF}}$ shows the actual expansion of the atoms. To determine the temperature, six images are taken at different times of flight t_{TOF}. Figure 6.2 shows the calculated squared widths σ^2 (variance) in dependence of the square of the time of flight. The slope of the fit to all datapoints (red line) equals, according to equation (6.1), σ_{v}^2, which is proportional to the temperature.

The error of the width of the atomic cloud is calculated in MATLAB and corresponds to the $68\,\%$-confidence interval of the applied fit.

Now we can calculate the temperature $T = 43.5 \pm 0.6\,\mu\text{K}$ corresponding to the slope of the fit $\sigma_{\text{v},1}^2/t_{\text{TOF}}^2 = 0.06017 \pm 0.00085\,\text{mm}^2/\text{ms}^2$ (red line) of Figure 6.2. This temperature can then be compared to the temperature T determined by the use of a simpler procedure where only two images at different times of flight are taken. The shorter time of flight, in which the atoms are not too dense so that stray light or wrongly-polarized light badly affects the determination of the atom number, will be the first point of interest ($t_{\text{TOF},1}$). The second one ($t_{\text{TOF},2}$) is reached when the atoms have had time to expand. With this, the temperature T is calculated by

$$T = \frac{\sigma_{\text{c}_2}^2 - \sigma_{\text{c}_1}^2}{t_{\text{TOF},2}^2 - t_{\text{TOF},1}^2} \frac{m}{k_{\text{B}}}. \tag{6.2}$$

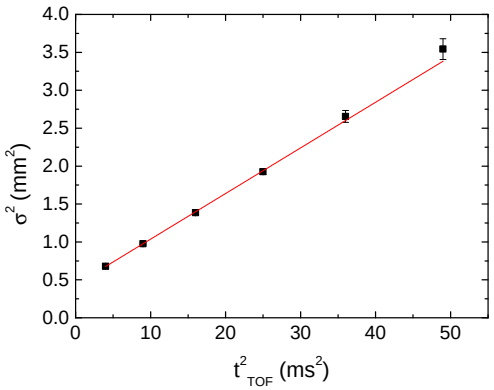

Figure 6.2. Time of flight measurement of an atomic cloud. The variance of a Gaussian fit σ^2 of images is depicted for different squared times of flight t_{TOF}^2. The red solid line corresponds to a linear fit to all data points.

In the results presented in this thesis, typical times of flight for atoms with a temperature of $T \approx 50\,\mu$K are $t_{\mathrm{TOF},1} = 2\,$ms and $t_{\mathrm{TOF},2} = 4\,$ms. The temperature of the atomic cloud for the corresponding values extracted from Figure 6.2 is $T = 42.6 \pm 1.1\,\mu$K. For the fact that this value is within the error of the temperature calculated by the linear fit, we will use the simpler procedure according to equation (6.2) to determine the temperature.

To determine the atom number N we sum over all the optical depths, which are determined by the fit function as shown in Figure 6.1 (b). If saturation effects of the atoms due to the light are negligible, the optical depth can be related to the atom density $\eta(x, y)$ as $\tau(x, y) = \eta(x, y)\sigma_{\mathrm{abs}}$ [42], where σ_{abs} is the absorption cross section[5]. With this we find the atom number

$$N = \sum_{x,y} \eta(x, y) \times u^2 = \sum_{x,y} \frac{\tau(x, y) \times (30.5\,\mu\mathrm{m})^2}{\sigma_{\mathrm{abs}}}. \tag{6.3}$$

by summing over the atom density and converting the pixel units to real length.

The contribution of multiple hyperfine levels in our imaging procedure prevents us from using the two-level absorption cross section to calculate the atom number. Therefore we have to find a conversion factor a_{c} for the real absorption cross section $\sigma_{\mathrm{abs}} = 3\lambda^2/(2\pi) \times a_{\mathrm{c}}$. In the FeLiKx experiment it is possible to determine the atom number by the use of another imaging method (see supplemental material of [14]). The discrepancy in atom number of both methods gives us a conversion factor of $a_{\mathrm{c}} = 2.4(1)$. The error of this factor influences all values in a same manner and is therefore not included into the error bars of the atom number. We can now multiply this conversion factor to the two-level absorption cross section and get $\sigma_{\mathrm{abs}} = 3\lambda^2/(2\pi) \times a_{\mathrm{c}}$. As a result of this measurement we obtain atom numbers after the MOT stage of $N_0 = 1.2 \times 10^8$.

The statistical error of the atom number is calculated via the error of the amplitude and the error of the standard deviation of the Gaussian fit to the data. In the following measurements, the atom number will be shown relative to the atom number measured after the magneto-optical

[5] It should be noted that the absorption cross section σ_{abs} is not related to the measured width of the atomic cloud σ.

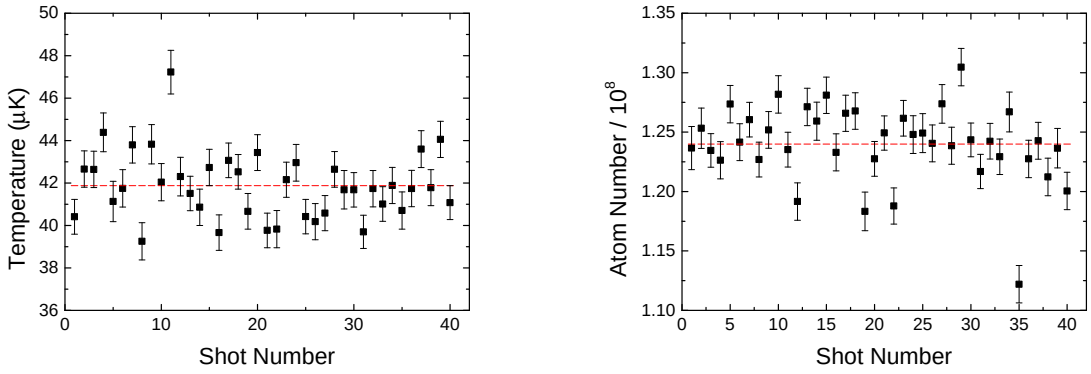

(a) **(b)**

Figure 6.3. Stability measurements. Panel (a) depicts the temperature and panel (b) depicts the atom number. Both plots are generated from the same set of data. The red dashed line indicates the mean value of temperature and atom number.

trap N_0. This is due to the fact that for the gray-molasses measurements, we are mainly interested in the cooled fraction N/N_0 of the atoms with respect to the atoms available at the end of the MOT stage.

To be certain that our experiment is stable and whether the errors - calculated by the program - are sufficiently big, 40 shots of the same measurement with the same parameters have been taken. Figure 6.3 depicts the resulting data points and their errors. The red dashed line illustrates the mean value. We observe that shot-to-shot fluctuations cause the atom number and the temperature to fluctuate by $\sim \pm 6\,\%$ around the mean value. A fraction of $45\,\%$ of the 40 temperatures are within the $68\,\%$ confidence interval of the mean value. We conclude that these error bars are not sufficiently big to cover shot-to-shot fluctuations. To compensate for the small error bars we multiply them by a factor of 2. To obtain similar results for the atom number we increase the error bars by a factor of 1.8 for the future data presentations.

To obtain the final results, the mean value for both dimensions is taken. If the cloud is Gaussian but with some angle θ relative to the imaging axes, the result of each direction may be different, but the mean value of both results gives the total temperature.

The initial cloud size $\sigma_0 = 0.66 \pm 0.01\,\text{mm}$ after the gray molasses is obtained by the linear fit of Figure 6.2. The size of the cloud after the MOT is $\sigma_{0,\text{MOT}} = 0.70 \pm 0.02\,\text{mm}$. There is no physical reason why the initial size after the MOT should be smaller than the initial size after the D1 molasses. A reason for these values might be that our atomic cloud is not perfectly Gaussian. An angle of Θ of the Gaussian with respect to the imaging axis could influence the calculations of the initial cloud size.

It should be noted that - in our experiment - for low intensities $I \leq 1.1\, I_{\text{SAT}}$ the atomic cloud starts to deform. The single Gaussian fit, which has been applied may not be the best fitting model [43]. Therefore the data achieved after shining a low-intensity molasses onto the atoms should be handled with care.

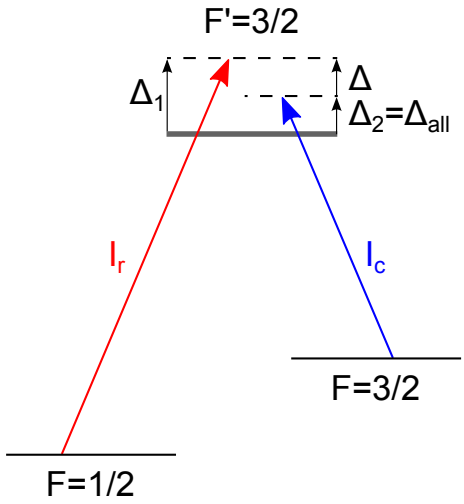

Figure 6.4. Laser configuration on the D1 transition of ^{6}Li. The red (blue) arrow labeled with I_r (I_c) depicts the repumper (cooler). This laser beam is detuned by Δ_1 (Δ_2) from transition frequency between the ground state $F = 1/2$ ($F = 3/2$) and the excited state $F' = 3/2$. The relative detuning between the repumper and the cooler is Δ. The overall detuning coincides with the detuning of the repumper $\Delta_\mathrm{all} = \Delta_2$.

6.2 Parameters for Sub-Doppler Cooling

The gray molasses cooling scheme is applied after the magnetic fields and laser beams of the Li-MOT are switched off fast $t < 100\,\mu$s. There is an additional waiting time $t_\mathrm{w} = 200\,\mu$s before the D1-molasses are turned on to assure that the magnetic fields can decay. As already explained in the previous chapter, this sub-Doppler cooling technique is operated at the D1-transition of ^{6}Li. The setup is built in a manner that many parameters can be varied to characterize the gray molasses and find the ideal operating point for our purposes.

The settings for the magnetic field can be tuned by varying the current through the compensation coils installed in the experiment. The absolute magnetic field at the position of the atoms cannot be measured using an external instrument and therefore the relative changes ΔB_x, ΔB_y, and ΔB_z outside the vacuum chamber will be stated. For the x and z direction of the magnetic field, the reference value is a current of $I_\mathrm{x} = I_\mathrm{z} = 0\,$A, whereas for the y direction it is $I_\mathrm{y} = 2\,$A. The magnetic field is measured by the FLUXMASTER Magnetometer from Stefan Mayer Instruments. The measured magnetic field has a linear dependence on the current in the measured range. The conversions are $\Delta B\mathrm{x} = 76.5 \pm 0.6\,\Delta I_\mathrm{x}$, $\Delta B\mathrm{y} = 187.7 \pm 0.8\,\Delta I_\mathrm{y}$ and $\Delta B\mathrm{z} = 343.6 \pm 1.2\,\Delta I_\mathrm{z}$. The estimated error of the measurement is $\pm 10\,$mG.

Figure 6.4 illustrates the two hyperfine ground states of ^{6}Li and the excited hyperfine state $F' = 3/2$. The laser beams used in this thesis to perform the gray-molasses cooling are labeled as I_r, the repump beam, and I_c, the cooling beam. Both of these beams are blue detuned with respect to the D1 transition of ^{6}Li. The detuning of the repumper is called Δ_1 and the detuning of the cooler is called Δ_2. The difference between the detuning of the laser beams is the relative detuning $\Delta = \Delta_1 - \Delta_2$. The detuning of the cooler can be varied separately by an AOM. The overall detuning Δ_all changes both Δ_1 and Δ_2 jointly. The detuning of the repumper can not be

varied separately and therefore coincides with the overall detuning. All of the detunings will be shown in units of the linewidth of the D1-transition $\Gamma = 2\pi \times 5.87\,\mathrm{MHz}$.

The intensity of the laser beams is expressed in terms of the saturation intensity of the D2-transition of ^{6}Li, namely $I_{\mathrm{SAT}} = 2.54\,\mathrm{mW/cm^2}$ [38]. In the measurements we will always state the intensity of one of the six beams. The intensity of the repumper (cooler) is labeled I_{r} (I_{c}) and is calculated by means of the peak intensity

$$I(0,z) = \frac{2P_0}{\pi\sigma_{\mathrm{i}}^2}, \tag{6.4}$$

in which P_0 is the measured power and σ_{i} the waist of the beam in horizontal $i = hor$ and vertical $i = ver$ direction.

The polarizations of the cooling and the repumping beam are linear. Due to the λ/4 plate that is installed in front of the retro-reflecting mirror, the co-propagating beams also have linear polarization, but perpendicular to the original beam. This configuration is called lin$\perp$lin ("lin perp lin") and is used in all measurements excpet the ones where it is stated otherwise.

6.3 Sub-Doppler Feature

The starting temperature for the D1-cooling stage is $T_{\mathrm{MOT}} = 225 \pm 7\,\mu\mathrm{K}$. To observe a cooling effect, the overall detuning is set to $\Delta_{\mathrm{all}} = 6\,\Gamma$, the intensities are set to values of $I_{\mathrm{c}} = 5.6\,I_{\mathrm{SAT}}$ and $I_{\mathrm{r}} = 0.44\,I_{\mathrm{SAT}}$, the molasses duration is $\tau_{\mathrm{M}} = 1\,\mathrm{ms}$ and the magnetic field settings are $\Delta B_{\mathrm{x}} = 260\,\mathrm{mG}$, $\Delta B_{\mathrm{y}} = 370\,\mathrm{mG}$, and $\Delta B_{\mathrm{z}} = 270\,\mathrm{mG}$.

Figure 6.5 (a) shows the atom number and temperature as the frequency of the cooling laser is varied. The frequency of the cooling laser is expressed in terms of the resulting detuning $\Delta = \Delta_2 - \Delta_1$ from the two-photon Raman condition. There appears to be a wide cooling feature at temperatures of $T \approx 110\,\mu\mathrm{K}$, which are well below the initial temperatures and also below the Doppler temperature of ^{6}Li.

At a closer region around the Raman condition, a feature that is narrower than the natural linewidth appears. In this regime, temperatures as low as $T \approx 40\,\mu\mathrm{K}$ at an atom fraction of near-unity can be achieved.

In the region of $0.25\,\Gamma < \Delta < 1.25\,\Gamma$ no images are plotted. The atoms have been at high temperatures. The resulting expansion of the atom cloud leads to a very low optical depth, resulting in low signal-to-noise in the absorption images. The two values $T = 565 \pm 182\,\mu\mathrm{K}$ ($0.37\,\Gamma$) and $T = 737 \pm 234\,\mu\mathrm{K}$ ($0.44\,\Gamma$) could be obtained but were not added to the Figure for the purpose of increased readability.

The comparison of the phase-space densities before ρ_{psd1} and after ρ_{psd2} the D1-cooling stage shows an improvement by a factor of

$$\rho_{\mathrm{psd2}}/\rho_{\mathrm{psd1}} = 14.6 \pm 2.3. \tag{6.5}$$

This means that we can increase the phase-space density of ^{6}Li by a factor of 15. An explanation for this efficient cooling is the formation of a dark state that is a coherent superposition of the two hyperfine ground states at $\Delta = 0$, at which the width of the cooling dip matches the width of the coherence, as theoretically described in [44].

Figure 6.5 (b) shows the temperature and Figure 6.5 (c) shows the cooled atom fraction at

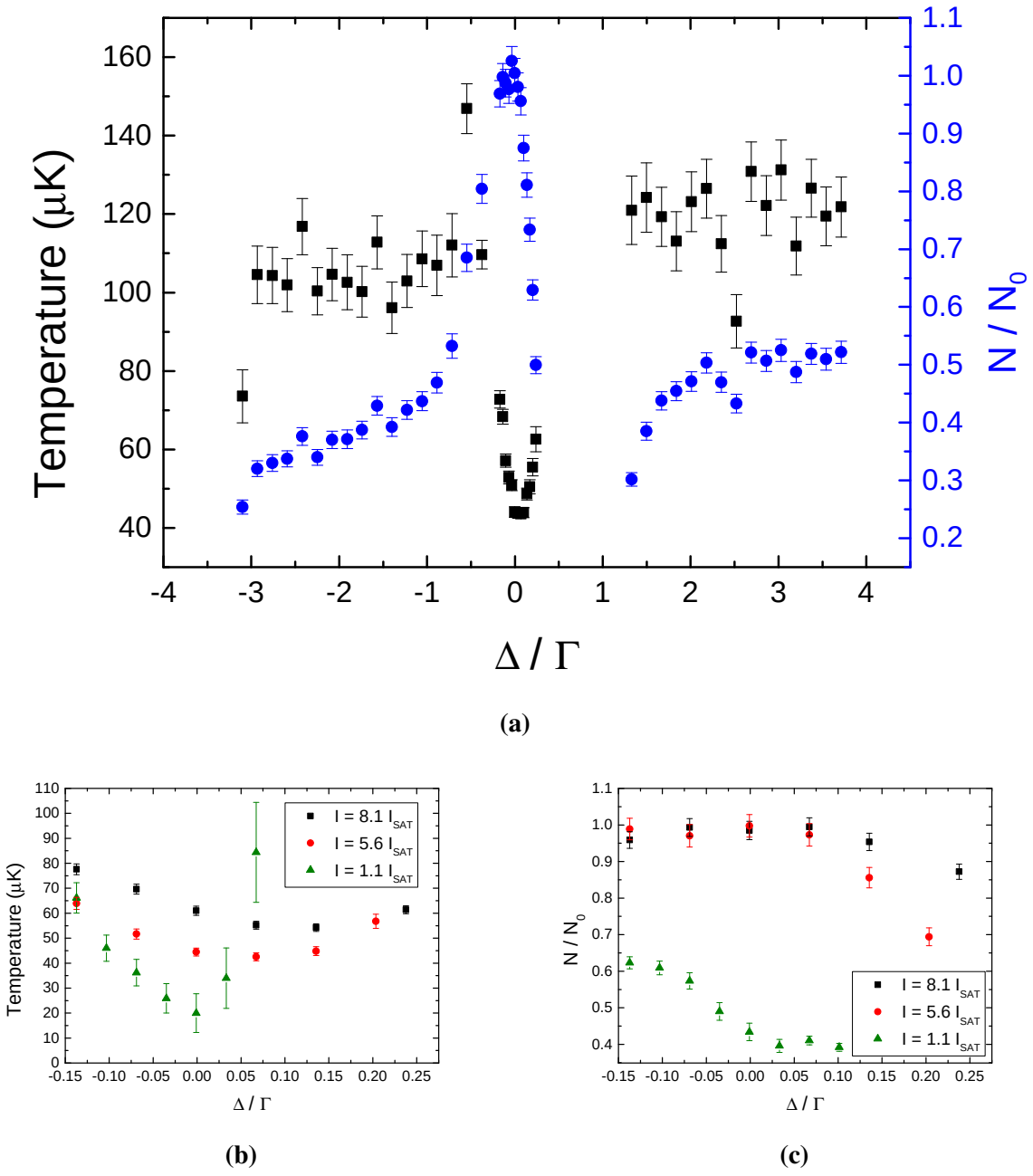

Figure 6.5. Dependence of temperature and atom fraction on the detuning of the repumper with respect to the cooler. Panel (a) shows this dependence for a wide range of repumper detunings. Panels (b) and (c) show the cooling region around the point $\Delta = 0$ for different beam intensities.

the cooling dip for different intensities. It can be seen that the higher (lower) the intensity, the higher (lower) are T and N/N_0. As already mentioned in section 6.1, the images taken at an intensity of $I_c = 1.1\, I_{SAT}$ are not fitted by the ideal model and therefore the error bars are greater than the error bars calculated for other intensities of the laser beams. The frequency setting at the Raman-condition is shifted to positive values as the intensity is increased. This occurrence can be interpreted as a different light shift resulting from different transition strengths of the involved states at different intensities.

The ideal operating point for the gray-molasses cooling seems to be at medium intensities $I_c = 5.6\, I_{SAT}$, at which temperatures of $T = 41.8 \pm 1.7\,\mu$K can be achieved, while keeping nearly all the atoms $N/N_0 = 0.98 \pm 0.04$ with respect to the MOT stage.

Many measurements are taken in a region near the Raman condition. For this purpose Δ_2 is kept at a fixed value and Δ_1 is varied. With such a configuration, a dataset can be taken around the value of $\Delta = \Delta_2 - \Delta_1 = 0$.

The detunings, intensities, magnetic field offsets and polarizations have been varied to find good settings for the gray molasses cooling scheme. The following sections describe the variation of one parameter at a time and therefore the others are fixed at values at which the lowest temperatures and highest atom numbers were found.

6.4 Dependence on Magnetic Field

In a previous publication [12] an influence of the magnetic field offset to the gray-molasses cooling scheme has been reported. Therefore we have varied the current through the compensation coils to vary the magnetic field offset. Detunings near the Raman condition $\Delta = 0$ are taken as the region of interest. Figures 6.7 (a) to (c) show the dependence of the temperature and the atom number on the offset magnetic filed in all three dimensions. The detunings are chosen to be $\Delta_{all} = 6\,\Gamma$ and $\Delta = 0.07\,\Gamma$ and the intensity is $I_c = 5.6\, I_{SAT}$. Two directions (e.g. x and y) have been kept at a fixed value whereas the other one (e.g. z) has been varied. These measurements show that the temperature varies by $\sim 40\,\mu$K if the magnetic field offset changes by $\sim 800\,$mG in z-direction. There is also a slight dependence in the y-direction, whereas the variation of ΔB_x does not seem to influence the temperature or the cooled fraction.

It can be seen that if all the other parameters are fixed, the magnetic field offset indeed has an influence on the temperature and on the atom number. One possible explanation for this effect is that the transition strength between the involved states changes by varying the B-field and therefore the frequencies, at which the Raman condition occurs, change.

The Figures 6.7 (a), (c), and (e) show the temperature and Figures 6.7 (b), (d), and (f) depict the cooled fraction at the cooling dip for different magnetic field offsets. In these measurements the magnetic field offsets of two directions have been kept fixed and a cooling dip for three magnetic field offsets of the third direction have been obtained. The fixed values are $\Delta B_x = 260\,$mG, $\Delta B_y = 370\,$mG, and $\Delta B_z = 270\,$mG. It can be seen that the points of lowest temperature shift in frequency as the magnetic field offset is changed. The temperatures and atom fractions of Figure 6.6 match the values of Figure 6.7 nicely, as one looks at a detuning of $\Delta = 0.07\,\Gamma$.

As a consequence of this measurement we fix the magnetic field offsets to $\Delta B_x = 260\,$mG, $\Delta B_y = 370\,$mG, and $\Delta B_z = 270\,$mG. The corresponding currents through the curvature coils

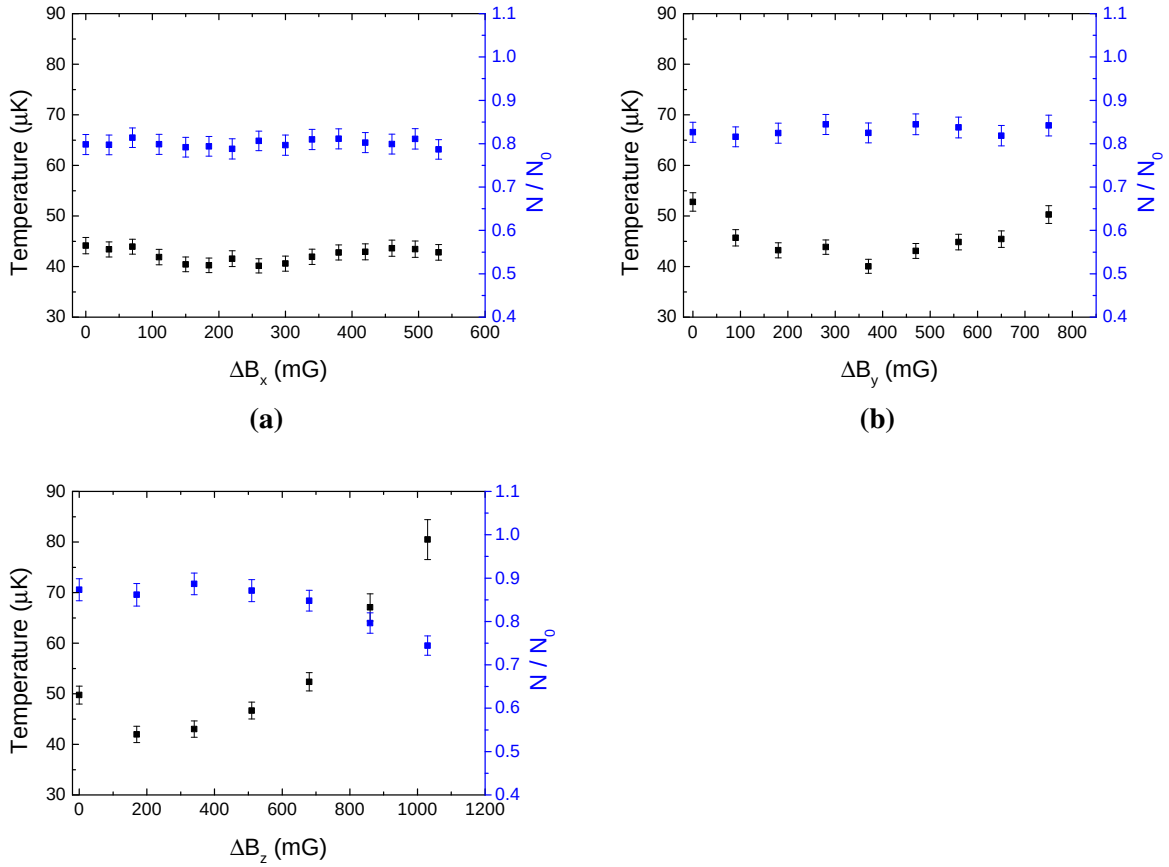

Figure 6.6. Temperature and atom fraction depending on the magnetic field offset in all three dimensions.

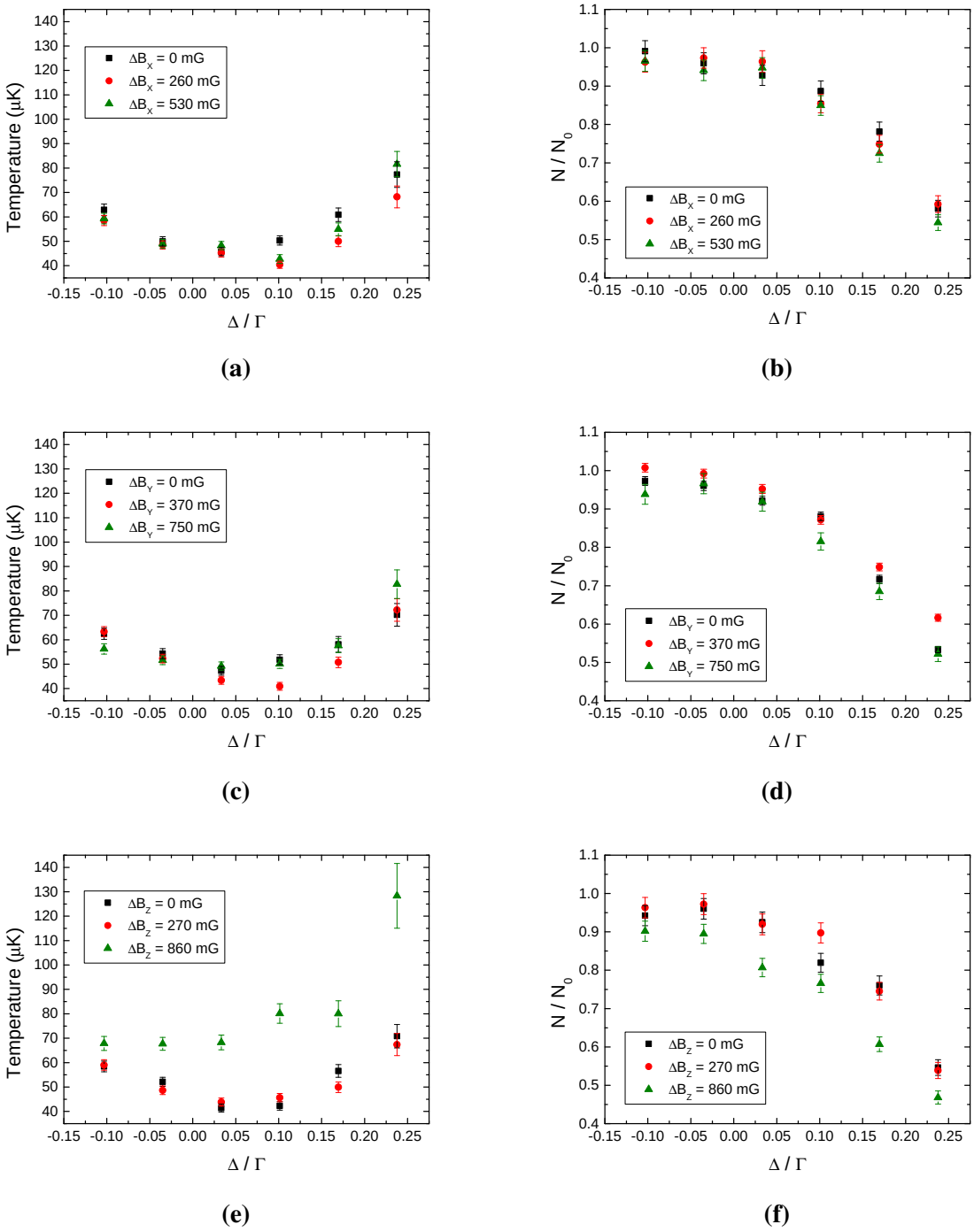

Figure 6.7. Figures (a),(c),(e): Temperature of cooling dip for different magnetic fields in x (top), y (middle), z (bottom) direction. Figures (b),(d),(f): Atom fraction at cooling dip for different magnetic fields in x (top), y (middle), z (bottom) direction.

are $I_x = 3.5\,\mathrm{A}$, $I_y = 4\,\mathrm{A}$, and $I_z = 0.8\,\mathrm{A}$.

6.5 Duration of Molasses

This section treats the dependence of the cooled fraction and the temperature of the atomic cloud while varying the duration of the molasses. For the intensity of $I_c = 5.6\,I_{SAT}$ ($I_c = 8.1\,I_{SAT}$, $I_c = 1.1\,I_{SAT}$) we have fixed the relative detuning $\Delta = 0.07\,\Gamma$ ($\Delta = 0.14\,\Gamma$, $\Delta = -0.03\,\Gamma$) and the overall detuning $\Delta_{all} = 6\,\Gamma$ ($\Delta_{all} = 6\,\Gamma$, $\Delta_{all} = 4.3\,\Gamma$).

Figure 6.8 (a) shows the dependence of the atoms' temperature on the molasses duration τ_M. We see that, for all the light intensities used in this work, for $\tau_M > 1\,\mathrm{ms}$, the temperature remains constant. Meanwhile, the number of atoms - depicted in Figure 6.8 (b) - in the molasses decreases with increasing τ_M. This decrease is faster at lower intensities. For shorter times the temperature slightly increases at a lower cooled fraction.

From these measurements we conclude that for medium intensity $I_c = 5.6\,I_{SAT}$ we can determine a sufficient molasses duration of $\tau_M = 1\,\mathrm{ms}$.

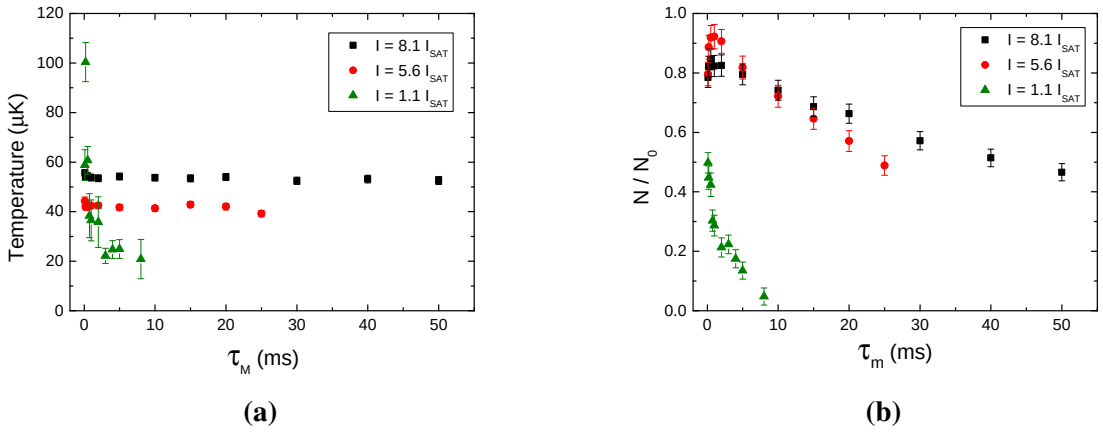

(a) **(b)**

Figure 6.8. Temperature (a) and atom fraction (b) as a function of molasses duration for three different intensities.

6.6 Repumper Intensity

The intensity of the repumper is another parameter whose eventual influence on the temperature or the atom fraction needs to be checked. It was varied from $0\,\%$ to $\sim 25\,\%$ of the intensity of the cooler. In Figure 6.9 it can be seen that no dependence is measured for ratios above $I_r/I_c \approx 0.05$. At this point it should be noted that there was an observation of the influence on the overall cooling effect of the gray-molasses technique, if the intensity of the repumper is increased to values higher than the cooler [44]. However, the intensities in this thesis have not been varied in that range. For further measurements we make sure that the intensity of the repumper does not exceed the intensity of the cooler.

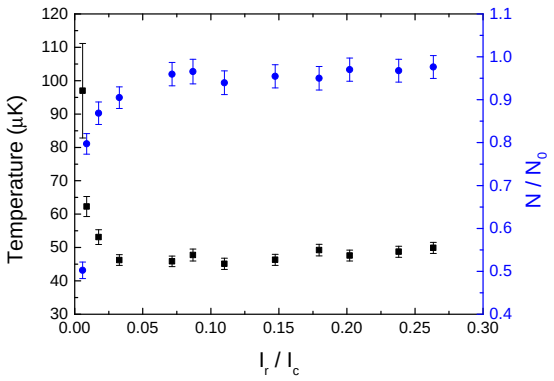

Figure 6.9. Temperature and atom fraction in dependence of the repumper intensity I_r. The intensity is stated relative to the cooler intensity I_c.

6.7 Overall Detuning

We also want to investigate the dependence of the cooled fraction and the temperature on the overall detuning. The relative frequency difference between the cooler and the repumper are kept at a fixed value $\Delta = 0.07\,\Gamma$ and the overall detuning Δ_all is varied. Figure 6.10 shows that in a range of $4\,\Gamma < \Delta_\mathrm{all} < 6\,\Gamma$ the temperature and the atom fraction do not change. At values closer to the resonance $\Delta_\mathrm{all} < 4\,\Gamma$ the temperature rises, which indicates that the lasers are not sufficiently blue detuned to reach as low temperatures as with a bigger detuning. At higher values $\Delta_\mathrm{all} > 6\,\Gamma$ the atom number decreases. This can be due to the fact that the AOM used to shift this frequency is driven at its outer limit, and therefore the intensity at the output drops.

Figure 6.11 shows the behavior of temperature (a) and cooled fraction (b) for different over-

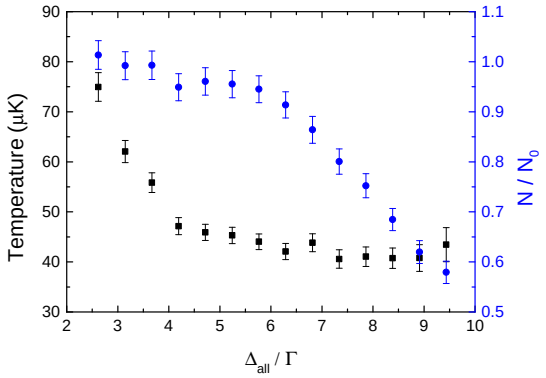

Figure 6.10. Temperature and atom number versus overall detuning Δ_all. The detuning is denoted in units of the linewidth Γ of the D1 transition in ^{6}Li.

all detunings dependent on the molasses duration. There is a similar behavior if it is compared to Figure 6.8. There, the low intensity $I_\mathrm{c} = 1.1\,I_\mathrm{SAT}$ regime behaves similarly to the high detuning regime which is an indicator that the output of the AOM is indeed lower at $\Delta_\mathrm{all} = 9.4\,\Gamma$. Measurements of another experiment [11] show that the temperature is increasing with high

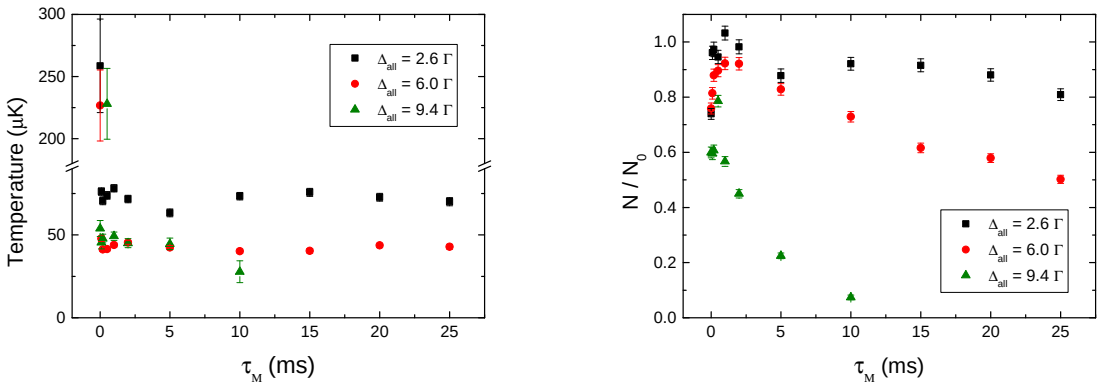

(a) **(b)**

Figure 6.11. Temperature (a) and atom fraction (b) with respect to the duration of the D1 molasses for three different overall detunings.

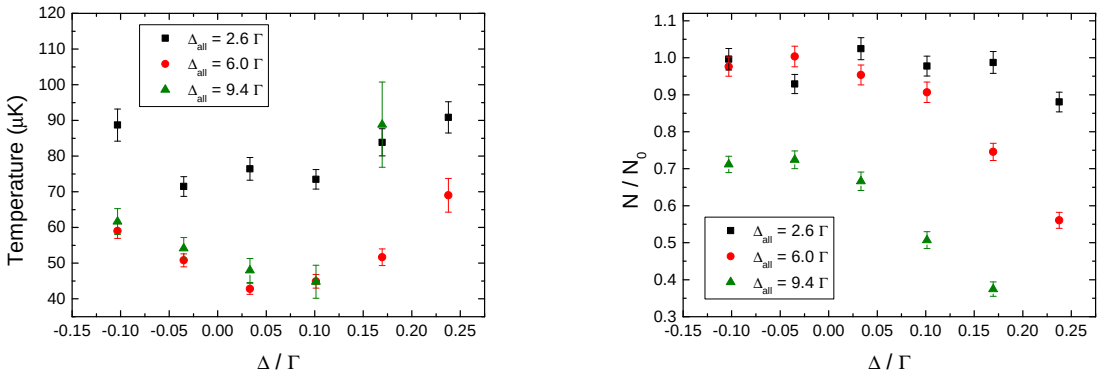

(a) **(b)**

Figure 6.12. Temperature (a) and atom fraction (b) at cooling dip for three different overall detunings.

detuning and the cooled fraction is relatively slowly decreasing. If the intensity is in fact lower, this will decrease the actual temperature.

We verify that the value of the relative detuning Δ at which the minimum temperature is obtained does not depend on the overall detuning. Figures 6.12 (a) and (b) show the temperature and atom fraction for three values of the overall detuning. With these measurements we can - similar to section 6.4 for the magnetic field offset - determine whether the change of Δ_{all} shifts each energy level differently and therefore shifts the detuning at which the Raman condition occurs. We do not observe any such shifts and conclude that at this intensity, the overall detuning will be fixed to $\Delta_{\text{all}} = 6\,\Gamma$ for future measurements.

6.8 Light Polarization

The choice of using a separate optical path for the D1 beams and for the MOT beams gives us the freedom to change the polarization of the cooling and repumping beams from linear to circular polarization. For this purpose the light output of the fiber at the main table is sent through a $\lambda/4$ plate. It then passes the atoms, is retro reflected and therefore passes the second $\lambda/4$ plate two times. If the quantization axis is chosen in propagation direction of the laser beams, the light is σ^+ and σ^- polarized. This polarization setting is called the $\sigma^+ - \sigma^-$ configuration. The previously presented measurements of this chapter are repeated with the new polarization setting. The fixed parameters in the following measurements are chosen as they were in the corresponding datasets for the lin⊥lin configuration.

In Figure 6.13 the variation of the overall detuning and the resulting changes in temperature

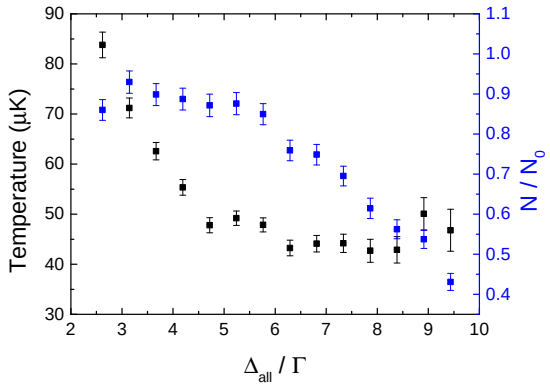

Figure 6.13. Temperature and atom number versus overall detuning Δ_{all}. The detuning is denoted in units of the linewidth Γ of the D1 transition in ^{6}Li.

and atom number are depicted. We observe similar behavior as in Figure 6.10 for the lin⊥lin configuration. The temperatures are slightly higher, and the atom number is lower if the laser beams are set to $\sigma^+ - \sigma^-$ configuration.

Figure 6.14 (a) shows the cooling feature resulting from the gray molasses in $\sigma^+ - \sigma^-$ configuration for detunings of $-3.1\,\Gamma < \Delta < 3.7\,\Gamma$. In the region of $-0.3\,\Gamma < \Delta < 1.2\,\Gamma$, the atoms have too high temperatures to be imaged. The wide cooling feature at about $\sim 130\,\mu$K shows a trend of slightly higher temperatures and a lower cooled fraction than what was observed, as the laser beams were set to the lin⊥lin configuration. The behavior of the cooling dip for different intensities is shown in Figures 6.14 (b) and (c). We observe similar trends, but a higher temperature at a lower cooled fraction compared to the values obtained in lin⊥lin configuration. In this measurement the medium intensities $I_c = 5.6\,I_{\text{SAT}}$ produce temperatures of $T = 45.5 \pm 1.5\,\mu$K at an atom fraction of $N/N_0 = 0.84 \pm 0.04$. With an initial cloud size of $\sigma_0 = 0.6243 \pm 0.0071$ mm, the resulting increase in phase-space density is $\rho_{\text{psd2}}/\rho_{\text{psd1}} = 13.0 \pm 3.3$.

Figure 6.15 shows the influence of the magnetic field offset in all directions on the temperatures and cooled atom fractions. From this measurement we conclude that the ideal settings are found at $\Delta B_x = 260$ mG, $\Delta B_y = 370$ mG, and $\Delta B_z = 270$ mG. The corresponding currents through the curvature coils are $I_x = 3.5$ A, $I_y = 4$ A, and $I_z = 0.8$ A. These values are

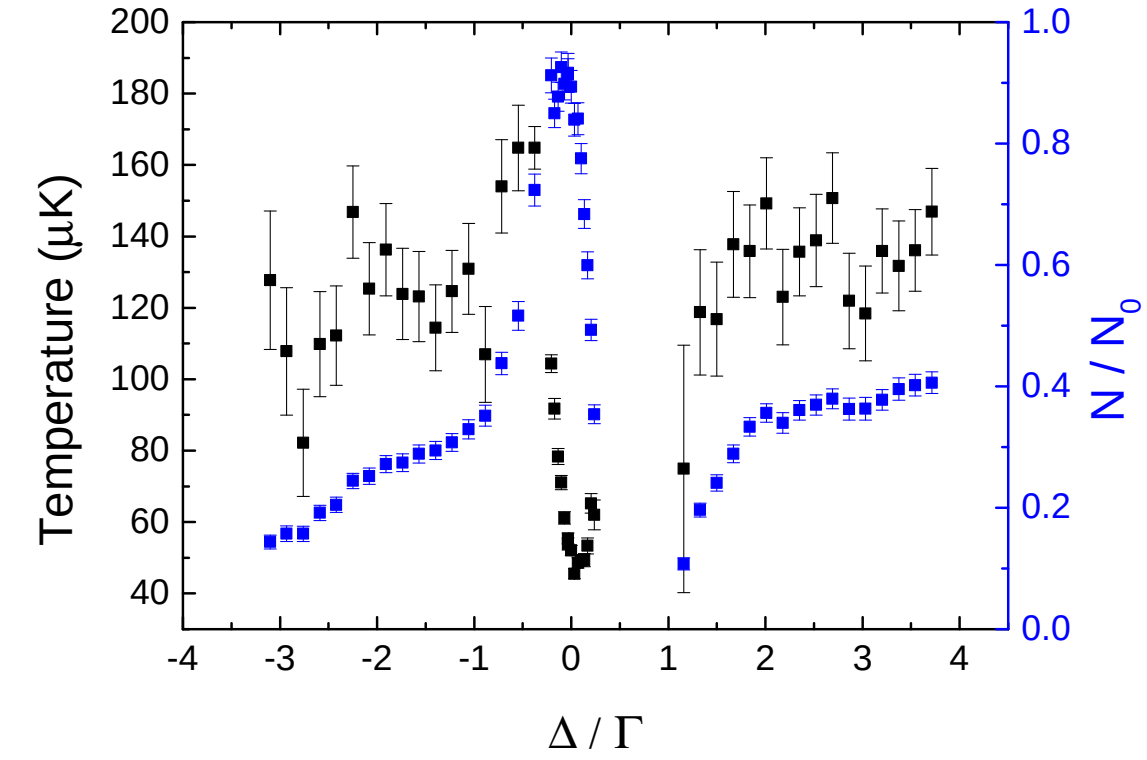

(a)

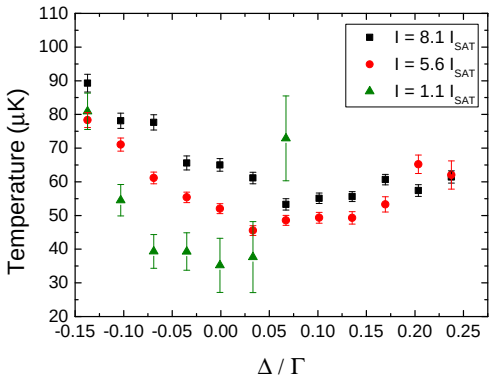

(b)

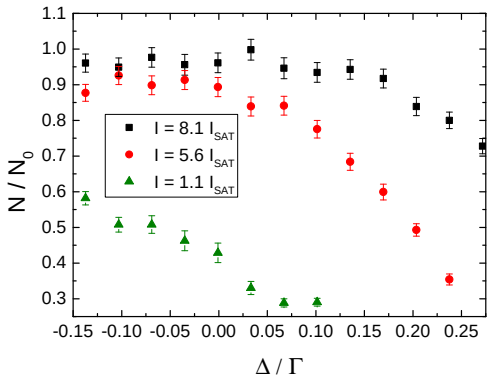

(c)

Figure 6.14. Dependence of temperature and atom fraction on the relative detuning Δ between the repumper and the cooler, for circularly polarized light. Figure (a) shows overall cooling feature in a wide range around $\Delta = 0$. Figures (b) and (c) show the temperature and the cooled fraction at the cooling dip for different beam intensities.

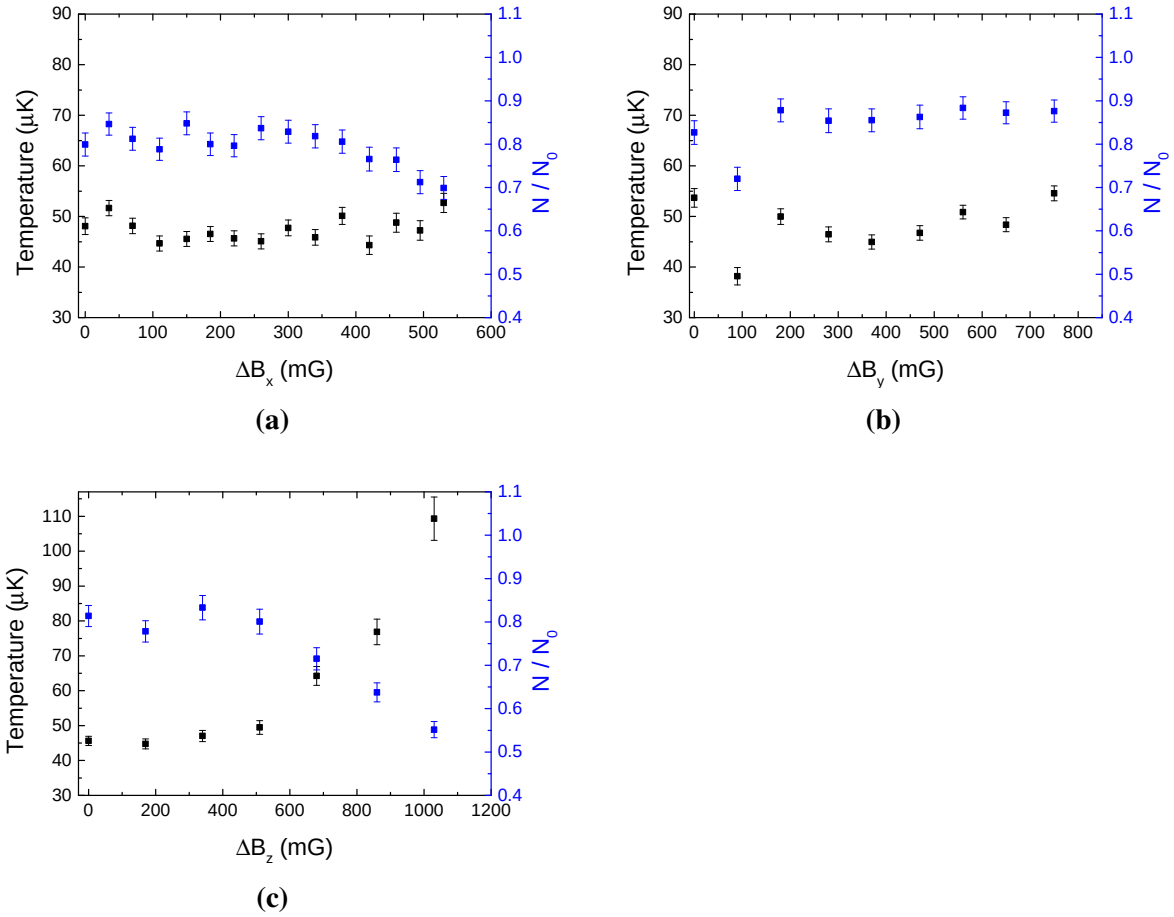

Figure 6.15. Temperature and atom fraction in dependence of the magnetic field offset. The magnetic fields are measured with respect to a current of $I = 0\,\mathrm{A}$ ($I = 2\,\mathrm{A}$) through the curvature coil in x, z direction (y direction).

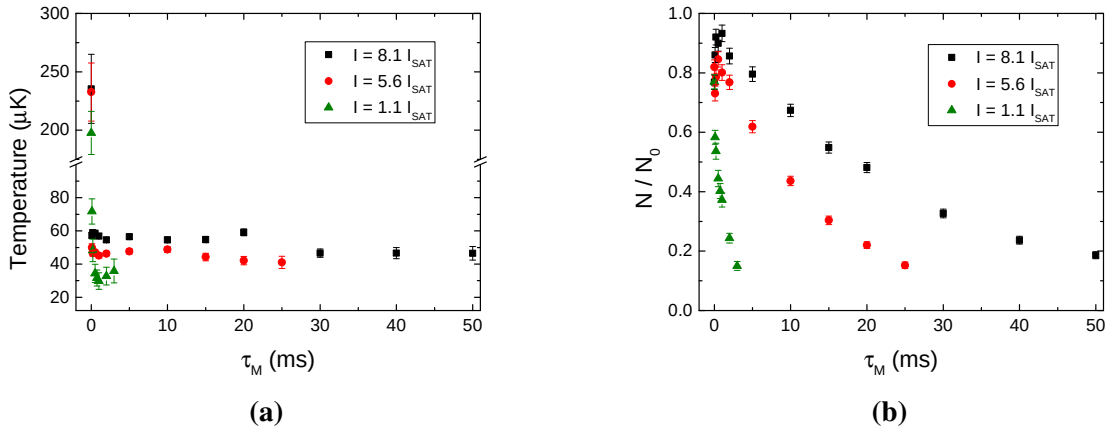

Figure 6.16. Temperature (a) and atom fraction (b) versus molasses time for three different intensities.

the same as for the lin⊥lin case.

The dependence of temperature and cooled fraction, on the molasses duration, for different intensities, is depicted in Figure 6.16. In this measurement we find best settings for medium intensities $I_c = 5.6\, I_{SAT}$ and a molasses time of $\tau_M = 1\,\text{ms}$.

6.9 Summary

In this chapter, the gray-molasses cooling scheme was characterized. The goal of the implementation of this system into the FeLiKx experiment was to improve the phase-space density by lowering the temperature while keeping the atom density as high as possible.

The gray-molasses technique worked best for our purposes in a medium intensity range $I = 5.6\, I_{SAT}$. At lower (higher) intensities we found a decrease (an increase) in temperature and atom number. The magnetic field offset showed an influence on the detuning at which the coldest point could be reached (Raman condition). Values were set to $\Delta B_x = 260\,\text{mG}$, $\Delta B_y = 370\,\text{mG}$, and $\Delta B_z = 270\,\text{mG}$. The duration of the molasses decreased cooled atom fraction, while the temperature stayed constant, for values of $\tau_M > 1\,\text{ms}$. For shorter times the temperature increased slightly and the cooled atom fraction decreased. Therefore the molasses duration was fixed to $\tau_M = 1\,\text{ms}$. The ratio between the intensity of the repumper and the cooler did not influence the cooling scheme in a range from $0 - 30\,\%$. The gray-molasses cooling showed no influence on the variation of the overall detuning in a range of $4\,\Gamma < \Delta_{all} < 6\,\Gamma$. We saw similar behavior for all these parameters as we changed the polarization from lin⊥lin to $\sigma^+ - \sigma^-$. The latter configuration produced samples with higher temperatures and lower cooled atom fraction.

The error bars shown in the data of this thesis do not include systematic errors. The systematic error of the temperature $\Delta T/T = \pm 6.5\,\%$ arises from the magnified pixel size $u = 30.5 \pm 1\,\mu\text{m}$. For the fact that the imaging beam is magnified on its way to the camera, the conversion from pixel units to real length differs from the one given by the datasheet of the camera. The error of the magnification factor and the error of the conversion factor $a_c = 2.4(1)$, which corrects for the two-level assumption in the imaging procedure, are contributing to an error of the absolute atom number and are not included into the error bars.

After the optimization of these parameters in the lin⊥lin configuration we observe a decrease in temperature from $T_{MOT} = 225 \pm 7\,\mu\text{K}$, after the MOT, to values as low as $T = 41.8 \pm 1.7\,\mu\text{K}$, after the sub-Doppler cooling stage. The cooled fraction at these temperatures is $N/N_0 = 0.98 \pm 0.04$. This corresponds to an increase in phase-space density by a factor of 14.6 ± 2.3. As these measurements are done, we switch our system to the $\sigma^+ - \sigma^-$ configuration. After optimization we find that this system favors the same parameter settings as in lin⊥lin configuration. The obtained temperatures of $T = 45.5 \pm 1.5\,\mu\text{K}$ are higher and the cooled fractions of $N/N_0 = 0.84 \pm 0.04$ are lower compared to the other polarization configuration. Nevertheless with these settings the phase-space density can be increased by a factor of 13.0 ± 3.3.

Chapter 7

Summary and Outlook

The goal of this thesis is to increase the phase-space density of a cloud of ^{6}Li atoms, precooled and confined in a MOT, using the gray-molasses technique on the D1 transition of lithium.

Chapter 2 presented an overview of laser cooling and the forces arising from the photon-atom interaction in a two-level atom. The absorption of photons by the atoms leads to a scattering force that - dependent on the light detuning - cools the atomic sample. By applying an optical molasses, an atomic cloud can be cooled to Doppler temperatures. This temperature limit arises from the balance between cooling effects that appear due to the absorption of photons, and heating effects, such as shot noise of the laser and the random motion of the atom due to spontaneous emission. We introduce the concept of phase-space density that is the comparison of the inter-particle distance and the thermal de Broglie wavelength. As this value approaches unity, effects of quantum statistics become important.

The consideration of the multi-level structure, introduced in the third chapter 3, opens the stage for explanations of other cooling mechanisms that lead to sub-Doppler temperatures. If the fine and hyperfine structure of an atom is considered, the polarization of the laser beam plays an important role. Due to the polarization of the light, different transitions in an atom can have different transition strengths. The Stark shift, arising from the interaction of the off-resonant laser beams with the atoms, shifts the energy levels of the atoms with different transition strengths differently. This is illustrated when considering the dressed-atom model, in which new eigenstates are found by diagonalizing the Hamiltonian and not treating the interaction as a perturbation, as was the case when deriving the optical-Bloch equations.

Chapter 4 explains the gray-molasses cooling scheme employs both, a sub-Doppler and a sub-recoil cooling effect. An atom is considered to move in a standing wave of blue-detuned laser beams. The atom can climb potential hills and roll them down again. If there appears optical pumping of states at the right position, the atom can be manipulated to just roll up and loose kinetic energy. This effect can be achieved by a polarization gradient and the right sign of the detuning. With the aid of this Sisyphus effect the temperature of an atomic sample can be reduced to a few recoil temperatures. Dark states are used to trap the atoms with velocity $v = 0$. If the Raman condition is fulfilled, a dark state will occur and the temperature can decrease to sub-recoil temperatures.

The optical setup for stabilizing the laser frequency and shifting the frequencies to values necessary for the gray-molasses cooling technique, is presented in chapter 5. With the aid of the modulation-transfer spectroscopy we stabilize the laser to the D1 transition of ^{6}Li. After that, the laser beam is split into the repumper and the cooling beam. Different AOMs are built up in single- and double-pass configuration to shift the frequencies of the two beams and to

make sure that the single beams are tunable over a few times the linewidth of the D1 transition. The prepared light is then sent through optical fibers to the trapping setup. Two beams in the horizontal and one in the vertical direction build up a three dimensional optical molasses within which the gray-molasses technique is realized. After the cooling procedure is done the atoms are imaged by absorption imaging using the time of flight method.

Chapter 6 presents the determination of temperature and atom number. After that the variable parameters are introduced. We varied the magnetic field, the time of molasses, the intensity of the repumper, and the overall detuning to find optimal values for operating the gray-molasses cooling. About $98\,\%$ of the atoms can be cooled to temperatures as low as $T = 41.8\,\mu$K. This means that the phase-space density can be increased by a factor of 14.6 ± 2.3 with respect to the value after the MOT. As a next step we change the polarization from lin$\perp$lin to $\sigma^+ - \sigma^-$ configuration. With the $\sigma^+ - \sigma^-$ polarized beams we can cool about $84\,\%$ of the atoms to temperatures of $T = 45.5\,\mu$K and achieve an increase in phase-space density by a factor of 13.0 ± 3.3.

A future step will be the implementation of the gray-molasses cooling into the experimental cycle of the FeLiKx experiment. In the current experimental setup, the atoms are precooled in a magneto-optical trap and then loaded into a single-beam optical dipole trap (ODT). A mixture of ^{6}Li atoms in the lowest two Zeeman states is evaporated at the magnetic field of $1150\,$G, on the attractive side of the $834\,$G ^{6}Li Feshbach resonance [45]. The potassium atoms are sympathetically cooled by the lithium atoms. After that, an interspecies Feshbach resonance can be used to investigate the interactions of the two atomic species. The interspecies resonance is located at a magnetic field of $154.7\,$G, which is on the repulsive side of the $834\,$G ^{6}Li Feshbach resonance. Changing the magnetic field from $1150\,$G to $154.7\,$G in the presence of Li atoms in both spin states leads to a large Li atom loss due to molecule formation. Therefore we eliminate all the atoms in one spin state by shining resonant light onto them at the magnetic field of $1150\,$G. Because of the large residual interactions between the Li atoms in the two spin states at $1150\,$G, this procedure also affects the other spin state and introduces heating.

The D1-cooling stage is already built into the experiment, but the major challenge is the loading of the atoms into the ODT. If we apply the gray-molasses cooling scheme, the cloud will be colder. Since the current depth of the ODT is much greater than $k_\mathrm{B}T_\mathrm{D1}$, the D1-cooled atoms will be heated while loading the ODT. To circumvent this problem we can decrease the trap depth by lowering the intensity of the single-beam ODT. This can be done by increasing the beam size and therefore also increasing the capture efficiency of the ODT.

A very important consequence of a larger beam diameter is a decrease of axial confinement of the atoms and the resulting strong increase in the particle loss. This problem can be solved by introducing a crossed-beam optical dipole trap. A crossed-beam trap has another big advantage. Higher atom densities are achievable and therefore it allows the evaporation of ^{6}Li atoms at a lower scattering length [46]. This would allow us to avoid the heating associated with the removal of one Li spin component and the ramping of the magnetic field across the Li Feshbach resonance.

Appendix A

Atom Light Interaction

A.1 Optical Bloch Equations

The following comprises a semi-classical treatment of the atom light interaction, where the atom is described using quantum mechanics, and the light field is classical. More precisely the deviation of the eigenfunction of the total Hamiltonian (atom plus light) will lead to the *optical Bloch equations*. These equations state the connection between the population of the atomic levels and the coherence of mixed states. The deviation is carried out on the basis of [21, 20]. The Hamiltonian of the whole system $\mathcal{H}$ is written as the sum of the field-free, time-independent Hamiltonian $\mathcal{H}_0$, and the interaction with the radiation field $\mathcal{H}'$.

$$\mathcal{H}\Psi(\mathbf{r},t) = (\mathcal{H}_0 + \mathcal{H}')\Psi(\mathbf{r},t) = i\hbar\frac{\partial\Psi(\mathbf{r},t)}{\partial t} \tag{A.1}$$

For simplicity the atom is assumed to have two levels. The eigenvalues and eigenfunctions of the unperturbed system can then be written as follows:

$$\mathcal{H}_0\Psi(\mathbf{r},t) = i\hbar\frac{\partial\Psi(\mathbf{r},t)}{\partial t} \tag{A.2}$$

$$\Psi_n(\mathbf{r},t) = \Psi_n(\mathbf{r})e^{-iE_nt/\hbar} \tag{A.3}$$

$$\mathcal{H}_0\Psi_1(\mathbf{r}) = E_1\Psi_1(\mathbf{r}) \tag{A.4}$$

$$\mathcal{H}_0\Psi_2(\mathbf{r}) = E_2\Psi_2(\mathbf{r}) \tag{A.5}$$

If the atom is driven by an external oscillating electric field, where $\mathcal{H}' = e\mathbf{r}\times\mathbf{E}_0\cos(\omega t)$ corresponds to the energy of an electric dipole $e\mathbf{r}$ in an oscillating electric field $\mathbf{E}_0\cos(\omega t)$, the wave function can be written as:

$$\Psi(\mathbf{r},t) = c_1(t)\Psi_1(\mathbf{r})e^{-iE_1t/\hbar} + c_2(t)\Psi_2(\mathbf{r})e^{-iE_2t/\hbar} \quad \text{with} \quad |c_1(t)|^2 + |c_2(t)|^2 = 1 \tag{A.6}$$

Inserting this wavefunction into the Schrödinger equation (A.1), a coupled differential equation for the coefficients $c_1(t)$ and $c_2(t)$ can be derived.

$$(\mathcal{H}_0 + \mathcal{H}')\Psi(\mathbf{r},t) = i\hbar\frac{\partial}{\partial t}(c_1(t)\Psi_1(\mathbf{r},t) + c_2(t)\Psi_2(\mathbf{r},t)) \tag{A.7}$$

$$\begin{aligned} i\dot{c}_1(t) &= \Omega\cos(\omega t)e^{-i\omega_0t}c_2 \\ i\dot{c}_2(t) &= \Omega^*\cos(\omega t)e^{i\omega_0t}c_1 \end{aligned} \tag{A.8}$$

The Rabi frequency Ω denotes the non vanishing integral $\langle 1|e\mathbf{r}\times\mathbf{E}_0|2\rangle/\hbar$, and $\omega_0 = (E_2 - E_1)/\hbar$ corresponds to the energy difference between the two states of the atom. When rewriting equations (A.8) to

$$\begin{aligned} i\dot{c}_1(t) &= \frac{\Omega}{2}(e^{i(\omega-\omega_0)t} + e^{-i(\omega+\omega_0)t})c_2 \\ i\dot{c}_2(t) &= \frac{\Omega^*}{2}(e^{-i(\omega-\omega_0)t} + e^{i(\omega+\omega_0)t})c_1 \end{aligned} \tag{A.9}$$

two terms of different frequencies appear. The $\omega + \omega_0$ term is oscillating fast and averages to zero, over some interaction time. Within the scope of the rotating-wave approximation, these terms are neglected and yield:

$$i\dot{c}_1(t) = \frac{\Omega}{2}e^{i(\omega-\omega_0)t}c_2, \text{ and } i\dot{c}_2(t) = \frac{\Omega^*}{2}e^{-i(\omega-\omega_0)t}c_1 \tag{A.10}$$

For the sake of future simplicity, the new variables

$$\begin{aligned} \tilde{c}_1 &= c_1\, e^{-i\frac{\Delta}{2}t}, \\ \tilde{c}_2 &= c_2\, e^{i\frac{\Delta}{2}t} \end{aligned} \tag{A.11}$$

are introduced. Finally the coefficients c_1 and c_2 take the form:

$$\begin{aligned} i\dot{\tilde{c}}_1 &= \frac{1}{2}(\Delta\tilde{c}_1 + \Omega\tilde{c}_2) \\ i\dot{\tilde{c}}_2 &= \frac{1}{2}(\Omega\tilde{c}_1 - \Delta\tilde{c}_2) \end{aligned} \tag{A.12}$$

To get a more intuitive picture of this mathematical deviation the density matrix ρ shall be introduced.

$$\rho = |\Psi(\mathbf{r},t)\rangle\langle\Psi(\mathbf{r},t)| = \begin{pmatrix} c_1(t)c_1^*(t) & c_1(t)c_2^*(t) \\ c_2(t)c_1^*(t) & c_2(t)c_2^*(t) \end{pmatrix} = \begin{pmatrix} \rho_{11} & \rho_{12} \\ \rho_{21} & \rho_{22} \end{pmatrix} \tag{A.13}$$

The entries of this matrix are of particular interest, because they are interpreted as physical properties of the atom. The diagonal elements denote the population of the states $|1\rangle$ and $|2\rangle$. The off-diagonal elements are referred to as the coherences of the mixed states. The optical Bloch equations, for coherent evolution of the states (no decay), can now be determined from equations (A.12) and (A.13).

$$\begin{aligned} \frac{\partial\rho_{11}}{\partial t} &= -\frac{\partial\rho_{22}}{\partial t} = i\frac{\Omega}{2}\left(\tilde{\rho}_{21} - \tilde{\rho}_{12}\right) \\ \frac{\partial\tilde{\rho}_{12}}{\partial t} &= \left(\frac{\partial\tilde{\rho}_{21}}{\partial t}\right)^* = -i\Delta\tilde{\rho}_{12} + i\frac{\Omega}{2}\left(\rho_{11} - \rho_{22}\right) \end{aligned} \tag{A.14}$$

If the decay of the excited state into the ground state with a rate Γ - which changes the population - is considered, the optical Bloch equations take following form:

$$\frac{\partial \rho_{11}}{\partial t} = \Gamma \rho_{22} + i\frac{\Omega}{2}\left(\tilde{\rho}_{21} - \tilde{\rho}_{12}\right) \tag{A.15}$$

$$\frac{\partial \rho_{22}}{\partial t} = -\Gamma \rho_{22} + i\frac{\Omega}{2}\left(\tilde{\rho}_{12} - \tilde{\rho}_{21}\right) \tag{A.16}$$

$$\frac{\partial \tilde{\rho}_{12}}{\partial t} = -\left(\frac{\Gamma}{2} + i\Delta\right)\tilde{\rho}_{12} + i\frac{\Omega}{2}\left(\rho_{11} - \rho_{22}\right) \tag{A.17}$$

$$\frac{\partial \tilde{\rho}_{21}}{\partial t} = -\left(\frac{\Gamma}{2} - i\Delta\right)\tilde{\rho}_{21} + i\frac{\Omega}{2}\left(\rho_{22} - \rho_{11}\right) \tag{A.18}$$

This are the equations of motion of the elements in the density matrix. They describe the dynamics of a two-level system. To get the steady state population of the excited sate ρ_{22} of an atom, one just needs to equate the time derivatives to zero and solve the system of equations. One then retrieves

$$\rho_{22} = \frac{\Omega^2/4}{\Delta^2 + \Omega^2/2 + \Gamma^2/4}. \tag{A.19}$$

Equation (A.19) shows that for a strong driving field ($\Omega \rightarrow \infty$), in a two level atom, the excited state population is 1/2.

A.2 Radiation Forces

This section comprises a treatment of the forces arising from the interaction of an atom in a near resonant laser field. The derivation is carried out on the basis of [20].

The force resulting from the atom-light interaction can be separated into a reactive and a dissipative part

$$F = F_{\text{sc}} + F_{\text{dip}}. \tag{A.20}$$

The dissipative force F_{sc}, discussed in detail in section 2.1, is also called the scattering force. The atom dissipates energy in form of a spontaneously emitted photon, which is used in Doppler-cooling. The reactive force F_{dip}, or dipole force, goes along with a potential in which atoms can be trapped. Both forces together build up the radiation forces.

The interaction energy U resulting from the laser induced dipole moment in an atom is given by

$$U = \frac{1}{2} e\mathbf{r}\mathbf{E}, \tag{A.21}$$

where $\mathbf{E} = E_0 \cos(\omega_{\text{L}} t - k_{\text{L}} r_{\text{L}})\hat{\mathbf{e}}_{\text{pol}}$ is the electric field of the laser with wavevector k_{L} and angular frequency ω_{L} propagating along an arbitrary direction $\mathbf{r}_{\text{L}}$ with arbitrary polarization $\hat{\mathbf{e}}_{\text{pol}}$. The derivative of the potential in equation (A.21) reveals the force

$$\mathbf{F} = -\nabla U = -eD_{\text{pol}}\left(\nabla E_0 \cos(\omega_{\text{L}} t - k_{\text{L}} r) + \frac{\mathbf{r}}{r} k E_0 \sin(\omega_{\text{L}} t - k_{\text{L}} r)\right), \tag{A.22}$$

acting on an atom. The induced dipole moment $e\mathbf{r}$ along the direction of the polarization $\hat{\mathbf{e}}_{\text{pol}}$ is given by the expectation value

$$-eD_{\text{pol}}(t) = -\int \Psi^{\dagger}(t) er \Psi(t) d^3\mathbf{r}. \tag{A.23}$$

With equation (A.6) one then obtains

$$D_{\text{pol}}(t) = c_2^* c_1 X_{12} e^{i\omega_0 t} + c_1^* c_2 X_{12} e^{-i\omega_0 t}. \tag{A.24}$$

The non-vanishing integral is denoted by X_{12}. Using the variables defined in equation (A.11) the displacement can be written as

$$D_{\text{pol}}(t) = X_{12}(u\cos(\omega_{\text{L}} t - k_{\text{L}} r) - v\sin(\omega_{\text{L}} t - k_{\text{L}} r)), \tag{A.25}$$

in which $u = \tilde{\rho}_{12} + \tilde{\rho}_{21}$ and $v = -i(\tilde{\rho}_{12} - \tilde{\rho}_{21})$. The force acting on the atoms

$$\bar{\mathbf{F}} = \left(\frac{\mathbf{r}}{r}\hbar k \frac{\Gamma\Omega^2}{4} - \frac{\hbar\Delta\Omega}{2}\nabla\Omega\right)\left(\frac{1}{\Delta^2 + \Omega^2/2 + \Gamma^2/4}\right) \tag{A.26}$$

is derived by calculating the steady state solutions for the coherence of the mixed states $\tilde{\rho}_{12}$ and $\tilde{\rho}_{21}$ - as done in equation (A.19) - and inserting equation (A.25) into equation (A.22). It should be noted that the $\bar{\mathbf{F}}$ is the time-averaged force over many oscillation periods. From equation A.26 one can read off the sum of a dissipative and a reactive force. These two forces describe the resonant and non-resonant optical excitation of an atom due to a photon, which are associated with cooling (dissipation of photons) and trapping (light shift) of atoms, respectively.

By taking the second summand of equation A.26 the dipole force

$$\mathbf{F}_{\text{dip}} = -\frac{\hbar\Delta}{2}\frac{\Omega}{\Delta^2 + \Omega^2/2 + \Gamma^2/4}\nabla\Omega \tag{A.27}$$

is derived. The first summand corresponds to the scattering force, as can be seen in equation (2.1).

Bibliography

[1] T.W. Hänsch and A.L. Schawlow. *Cooling of gases by laser radiation*, Opt. Comm. **13**, 1 (1975).

[2] S.V. Andreev, V.I. Balykin, V.S. Letokhov, and V.G. Minogin. *Radiative slowing and reduction of the energy spread of a beam of sodium atoms to 1.5 K in an oppositely directed laser beam*, Pis'ma Zh. Eksp. Teor. Fiz. 34, 463 [JETP Lett. **34**, 442 (1981)].

[3] S. Chu, L. Hollberg, J.E. Bjorkholm, A. Cable, and A. Ashkin. *Three-dimensional viscous confinement and cooling of atoms by resonance radiation pressure*, Phys. Rev. Lett. **55**, 48 (1985).

[4] E.L. Raab, M. Prentiss, A. Cable, S. Chu, and D.E. Pritchard. *Trapping of neutral sodium atoms with radiation pressure*, Phys. Rev. Lett. **59**, 2631 (1987).

[5] D.J. Wineland, R.E. Drullinger, and F.L. Walls. *Radiation-pressure cooling of bound resonant absorbers*, Phys. Rev. Lett. **40**, 1639 (1978).

[6] W. Neuhauser, M. Hohenstatt, P. Toschek, and Dehmelt H. *Optical-sideband cooling of visible atom cloud confined in parabolic well*, Phys. Rev. Lett. **41**, 233 (1978).

[7] V.S. Letokhov, V.G. Minogin, and B.D. Pavlik. *Cooling and trapping of atoms and molecules by a resonant laser field*, Zh. Eksp. Teor. Fiz. **72**, 4 (1977) [Sov. Phys.JETP **45**, 698-705 (1977)].

[8] E. Wille. *Preparation of an optically trapped Fermi-Fermi mixture of ^{6}Li and ^{40}K atoms and characterization of the interspecies interactions by Feshbach spectroscopy*. PhD thesis, Institut für Quantenoptik und Quanteninformation, 2009.

[9] M. Jag, M. Zaccanti, M. Cetina, R. S. Lous, F. Schreck, R. Grimm, D. S. Petrov, and J. Levinsen. *Observation of a strong atom-dimer attraction in a mass-imbalanced Fermi-Fermi mixture*, Phys. Rev. Lett. **112**, 075302 (2014).

[10] C. Kohstall, M. Zaccanti, M. Jag, A. Trenkwalder, P. Massignan, G. M. Bruun, F. Schreck, and R. Grimm. *Metastability and coherence of repulsive polarons in a strongly interacting Fermi mixture*, Nature **485**, p. 615-618 (2012).

[11] A. Burchianti. *Efficient all-optical production of large ^{6}Li quantum gases using D_1 gray-molasses cooling*, Phys. Rev. A **90**, 043408 (2014).

[12] A. T. Grier, I. Ferrier-Barbut, B. S. Rem, M. Delehaye, L. Khaykovich, F. Chevy, and C. Salomon. *λ-enhanced sub-Doppler cooling of lithium atoms in D1 gray molasses*, Phys. Rev. A **87**, 063411 (2013).

[13] C. Chin, R. Grimm, P. Julienne, and E. Tiesinga. *Feshbach resonances in ultracold gases*, Rev. Mod. Phys. **82**, 1225 (2010).

[14] M. Cetina, M. Jag, R.S. Lous, J.T.M. Walraven, R. Grimm, R.S. Christensen, and G.M. Bruun. *Decoherence of impurities in a Fermi sea of ultracold atoms*, arXiv:1505.00738 (2015).

[15] J. Levinsen, T.G. Tiecke, J.T.M. Walraven, and D.S. Petrov. *Atom-dimer scattering and long-lived trimers in fermionic mixtures*, Phys. Rev. Lett. **103**, 153202 (2009).

[16] M. Knap, A. Shashi, Y. Nishida, A. Imambekov, D.A. Abanin, and E. Demler. *Time-dependent impurity in ultracold fermions: orthogonality catastrophe and beyond*, Phys. Rev. X **2**, 041020 (2012).

[17] W.V. Liu and F. Wilczek. *Interior gap superfluidity*, Phys. Rev. Lett **90**, 4 (2003).

[18] M. Iskin and C.A.R. Sá de Melo. *Two-species fermion mixtures with population imbalance*, Phys. Rev. Lett. **97**, 100404 (2006).

[19] R.B. Diener and M. Randeria. *BCS-BEC crossover with unequal-mass fermions*, Phys. Rev. A **81**, 033608 (2010).

[20] C.J. Foot. *Atomic physics*. OXFORD University Press, 2011.

[21] H.J. Metcalf and P. van der Straten. *Laser cooling and trapping*. Springer, 1999.

[22] C.G. et al Townsend. *Phase-space density in the magneto-optical trap*, Phys. Rev. A **52**, 2 (1995).

[23] O. J. Luiten, M. W. Reynolds, and J. T. M. Walraven. *Kinetic theory of the evaporative cooling of a trapped gas*, Phys. Rev. A **53**, 381 (1996).

[24] R. Eisberg and R. Resnick. *Quantum physics of atoms, molecules, solids, nuclei and particles*. John Wiley & Sons Inc., 2nd edition, 1985.

[25] B.E.A. Saleh and M.C. Teich. *Fundamentals of photonics*. Wiley, 2007.

[26] A. M. Ellis. *Spectroscopic selection rules: the role of photon states*, J. Chem. Ed. **76**, 9 (1999).

[27] R. Grimm, M. Weidemüller, and Y. B. Ovchinnikov. *Optical dipole traps for neutral atoms*, arXiv:physics/9902072v1 (1999).

[28] B. E. King. *Angular momentum coupling and rabi frequencies for simple atomic transition*, arXiv:0804.4528v1 (2008).

[29] C.C. Tannoudji and J.Dalibard. *The new physics for the twenty-first century, Manipulating atoms with photons*. Cambridge University Press.

[30] G. Salomon, L. Fouché, P. Wang, A. Aspect, P. Bouyer, and T. Bourdel. *Gray-molasses cooling of ^{39}K to a high phase-space density*, Eur. Phys. Lett. **104**, 63002 (2013).

[31] D. Boiron, A. Michaud, P. Lemonde, Y. Castin, C. Salomon, S. Weyers, K. Szymaniec, L. Cognet, and A. Clairon. *Laser cooling of cesium atoms in gray optical molasses down to 1.1 μK*, Phys. Rev. A **53**, R3734 (1996).

[32] J. Dalibard and C. C. Tannoudji. *Dressed-atom approach to atomic motion in laser light: the dipole force revisited*, J. Opt. Soc. Am. B **2**, 1707 (1985).

[33] C. C. Tannoudji. *Manipulating atoms with photons*, Rev. Mod. Phys. **70**, 3 (1998).

[34] Y. Castin, J. Dalibard, and C.C. Tannoudji. *The limits of Sisyphus cooling*. Laboratoire de Spectroscopie Hertzienne de L'Ecole Normale Supérieure and Collége de France, 24, Rue Lhomond, F-75231 Paris Cedex 05, France.

[35] J. Dalibard and C. C. Tannoudji. *Laser cooling below the Doppler limit by polarization gradients: simple theoretical models*, J. Opt. Soc. Am. B **6**, 11 (1989).

[36] C. C. Tannoudji. *Dark resonances. From optical pumping to cold atoms and molecules*. Collége de France and Laboratoire Kastler Brossel, Département de Physique de l'Ecole Normale Supérieure, 24 rue Lhomond F - 75231 Paris Cedex 05, 2009.

[37] E. Arimondo and G. Orriols. *Nonabsorbing atomic coherences by coherent two-photon transition in a three-level optical pumping*, Lettere al Nuovo Cimento **17**, 10 (1976).

[38] Michael E. Gehm. Properties of ^{6}li. licenced by: http://creativecommons.org/licenses/by-nc-sa/1.0.

[39] P. D. Lett, R. N. Watts, C. I. Westbrook, and W. D. Phillips. *Observation of atoms laser cooled below the Doppler limit*, Phys. Rev. Lett. **61**, 2 (1988).

[40] J.H. Shirley. *Modulation transfer processes in optical heterodyne saturation spectroscopy*, Opt. Lett. **7**, p. 537-539 (1982).

[41] F. Träger. *Springer handbook of laser optics*. Springer, 2012.

[42] T. Pyragius. *Developing and building an absorption imaging system for ultracold atoms*, arXiv:1209.3408v3 (2012).

[43] J. Jersblad, H. Ellmann, K. Støchkel, A. Kastberg, L. Sanchez-Palencia, and R. Kaiser. *Non-Gaussian velocity distributions in optical lattices*, Phys. Rev. A **69**, 013410 (2004).

[44] F. Sievers, N. Kretzschmar, D.R. Fernandes, D. Suchet, M. Rabinovic, S. Wu, C.V. Parker, L. Khaykovich, C. Salomon, and F. Chevy. *Simultaneous sub-Doppler laser cooling of fermionic ^{6}Li and ^{4}0K on the D_1 line: theory and experiment*, Phys. Rev. A **91**, 023426 (2015).

[45] F.M. Spiegelhalder, A. Trenkwalder, D. Naik, G. Kerner, E. Wille, G. Hendl, F. Schreck, and R. Grimm. *All-optical production of a degenerate mixture of ^{6}Li and ^{4}0K and creation of heteronuclear molecules*, Phys. Rev. A **81**, 043637 (2010).

[46] M. Duarte, R.A. Hart, J.M. Hitchcock, T.A. Corcovilos, T.L. Yang, A. Reed, and R.G. Hulet. *All-optical production of a lithium quantum gas using narrow-line laser cooling*, Phys. Rev. A **84**, 061406(R) (2011).